Science
AAAS

Supplementary Materials for

Aster-dependent nonvesicular transport facilitates dietary cholesterol uptake

Alessandra Ferrari *et al*.

Corresponding author: Peter Tontonoz, ptontonoz@mednet.ucla.edu

Science **382**, eadf0966 (2023)
DOI: 10.1126/science.adf0966

The PDF file includes:

Materials and Methods

Mice

Aster-B global knock out mice were described before (*25*). Aster-C global knock out mice were obtained from MMRRC (C57BL/6N-Atm1Brd *Gramd1*ctm1a(KOMP)Wtsi/JMmucd). The mutation was induced by insertion of the L1L2_Bact_P cassette at position 43812106 of Chromosome 16 upstream of the critical exon (exon 11). *Gramd1*b$^{fl/fl}$ mice were generated by C57BL/6 ES cell-based gene targeting. Briefly, exons 3-6 of the macrophage variant (exons 6-9 of intestine specific variant) were selected as conditional knockout region. To engineer the targeting vector, homology arms and conditional KO region were generated by PCR using BAC clone RP23-366E16 and RP23-184D8 from the C57BL/6 library as template. In the targeting vector, the Neo cassette was flanked by SDA (self-deletion anchor) sites. Aster-C $^{fl/fl}$ mice were generated from C57BL/6N-Atm1Brd *Gramd1*ctm1a(KOMP)Wtsi/JMmucd. The cassette is composed of an FRT site followed by lacZ sequence and a loxP site. This first loxP site is followed by a neomycin resistance gene under the control of the human beta-actin promoter, SV40 polyA, a second FRT site, and a second loxP site. A third loxP site is inserted downstream of exon 11 at position 43812967. Exon 11 is thus flanked by loxP sites. The floxed allele was created by flp recombinase expression in mice carrying this allele. *Gramd1*b$^{fl/fl}$, *Gramd1*c$^{fl/fl}$ and *Gramd1*b$^{fl/fl}$*Gramd1*c$^{fl/fl}$ mice were backcrossed into C57BL/6NTac (Taconic) background and crossed with Villin-CreERT2 (B6.Cg-Tg(Vil1-cre/ERT2)23Syr/J, RRID:IMSR_JAX:020282) mice to generate tamoxifen-inducible intestine-specific knockout. After consecutive intraperitoneal injections of 1 mg tamoxifen in 100 µl corn oil for 5 days, intestine-specific knockouts were generated. 3×HA Aster-B knock-in mice were generated on a C57BL/6NTac (Taconic) background by inserting a 3×HA tag into the first exon of *Gramd1b* gene using a CRISPR/Cas9 based strategy (3XHA sequence flanked by ~50 bp homology arms: TATCCATACGATGTTCCTGACTATGCGGGCTATCCCTATGACGTCCCGGACTATGCAGGATCG TATCCTTATGACGTTCCAGATTACGCT). NPC1L1-knockout mice were a gift from Bao Liang Song, Wuhan University. They were also backcrossed to 3×HA Aster-B knock-in mice. For the in vivo kinetic absorption of radiolabeled cholesterol in the presence of ezetimibe or AI-3d, 8-week-old female mice (C57BL/6J, RRID:IMSR_JAX:000664) were purchased from The Jackson Laboratory.

For gene expression, protein expression, and lipidomic analyses small intestines were excised and flushed with 50 mL of ice-cold phosphate buffered saline (PBS) supplemented with protease inhibitor cocktail (Roche) and with 1 mM dithiothreitol (DTT). Small intestines were cut into three segments with length ratios of 1:3:2 (corresponding to duodenum, jejunum, and ileum), and each segment was opened longitudinally and scraped with ice-cold glass to isolate scrapings containing intestinal epithelial cells. Intestinal scrapings were snap frozen in liquid nitrogen and stored at -80°C or fixed in 10% formalin for histological analysis. Unless otherwise specified, duodenum was used for protein detection, proximal jejunum for lipidomic analysis, and distal jejunum for gene expression analysis. Blood was collected by cardiac puncture (terminal) or by retro-orbital bleeding, and the plasma was separated by centrifugation. Unless otherwise specified, mice were fed chow diet ad libitum and housed in a pathogen-free animal facility at 22°C, with a daylight cycle from 06:00 to 18:00. For western diet high cholesterol studies, male mice were fed a western diet containing 1.25% cholesterol (Research Diet, D09062501Ni) for 21 days. At the end of the study mice were fasted for 4 h before the euthanasia. Male mice were also used to investigate the effects of the NPC1L1 inhibitor ezetimibe on mice with deletion of Asters. In this regard, mice were fed for 3 days with a control diet containing 830 mg/kg cholesterol or with a matched diet containing 0.01% ezetimibe. Mice were fasted overnight and refed for 2 h before the euthanasia. All animal experiments were approved by the UCLA Institutional Animal Care and Research Advisory Committee.

Histology and Immunohistochemistry

For histology, fragments of jejunum were fixed overnight in 10% neutral-buffered formalin at room temperature, embedded in paraffin, and sectioned. Sections were deparaffinized and stained with H&E. For HA-Aster-B immunohistochemistry, 3×HA Aster-B mice were fed for 3 days with Ctrl diet or EZ diet and were treated three times (every 12 h) by oral gavage with 40 mg/kg GW3965. After the last administration of GW3965, mice were fasted for 4 h and then orally administered vehicle or 10 mg/kg ezetimibe 30 min before receiving a gastric gavage with corn oil only, or corn oil containing 6 mg of cholesterol. After 1 h, mice were euthanized and perfused with 10 ml cold HBSS. Small intestines were dissected, and intestinal lumen was immediately flushed with 20 ml cold HBSS to fully remove luminal content, followed by slow perfusion with 10 ml of cold neutral buffered formalin for immediate fixation of the villi. Small intestine was longitudinally opened and Swiss-rolling of the intestine was

performed from duodenum to distal ileum, with villus tip facing radially outwards. Intestine Swiss roll was then immobilized with foam biopsy pads in histology macro-cassette and fixed for 48 h in formalin followed by dehydration in 70% ethanol. Tissue was paraffin-embedded, and 5 µm cross-sections were obtained to reveal the entire roll face. Sections were deparaffinized and subjected to antigen retrieval with 10 mM sodium citrate (pH 6.0) in a sub-boiling water bath for 20 min. Slides were then incubated with the primary antibody (Table S1) overnight at 4°C. For IHC staining, slides were further incubated with Envision+ System-HRP Labelled Polymer Anti-Rabbit (Agilent, # K400311-2) at room temperature for 1 h and developed with ImmPACT DAB Peroxidase (HRP) Substrate (Vector, #SK4105).

Cholesterol absorption assays

For the acute cholesterol uptake assay, female mice were fasted for 4 h and then gavaged with 2 µCi [^{14}C] cholesterol (Perkin Elmer) in 200 µl olive oil. 2 h later, mice were euthanized and small intestine was excised (between the base of the stomach and the cecal junction), flushed with 0.5 mM sodium taurocholate in PBS, and cut it into 2-cm segments, as previously described (*44*). Segments were incubated with 500 ml of 1N NaOH at 65°C overnight and mixed with ScintiSafe (Fisher Scientific), and scintillation was counted. Plasma and liver were also harvested, and liver large lobes were incubated with 1 mL of 1N NaOH at 65°C overnight and mixed with ScintiSafe for scintillation counting.

For the acute fatty acid uptake assay, the mice were fasted for 4 h and then gavaged with 2 µCi [^{14}C] triolein in 200 µl olive oil. The samples were processed as described above.

Cholesterol absorption was also measured in kinetic assays where mice were fasted for 10 h and then gavaged with 2 µCi [^{14}C] cholesterol in 200 µl olive oil. Blood was collected at time 0, 30 min, 1, 2, 4, 6, and 12 h, and the plasma was separated by centrifugation. Radioactivity was measured by scintillation.

For studies in the presence of Poloxamer-407, 10 g of Poloxamer-407 were resuspended in 100 mL of 0.9% NaCl saline and stirred overnight at 4°C. 10 mL/g of body weight was administered by intraperitoneal injection right before the oil gavage with 2 µCi [^{14}C] cholesterol. Blood was collected at time 0, 1, 2, 3, and 4 h, and the plasma was separated by centrifugation. Radioactivity was measured by scintillation.

Fractional cholesterol absorption was measured by fecal dual isotope as previously described (*24*). Briefly, the mice were gavaged with 100 µl corn oil containing 0.5 µCi [^{14}C] cholesterol µCi, 1 µCi [^{3}H] sitostanol (American Radiolabeled chemicals), and 0.1 mg unlabeled cholesterol. Total fecal output was collected for 72 h, snap frozen, and pulverized using a pestle and a mortar. 500 mg of pulverized feces were used for lipid extraction (*45*) with 19 volumes of 2:1 (v/v) chloroform:methanol at 60°C for 3 min. The insoluble material was pelleted by centrifugation (1000*g* for 5 min at 4°C). The chloroform:methanol extraction was repeated on the insoluble material. S olvent was removed by drying under N_2 gas. Extracted lipids were saponified with 3 mL of 1:1 (v/v) methanol:2N NaOH(aq) for 60 min in a 60°C water bath. The neutral sterols were isolated with 3 sequential petroleum ether extractions, by adding 3 mL of petroleum ether to each tube, mixing vigorously, and separating the phases by centrifugation (1000*g* for 5 min at 4°C). The upper, organic, phase was transferred to a scintillation vial. The contents of the scintillation vials were dried under N_2 prior to addition of scintillation cocktail. The radioactivity was quantified by liquid scintillation counting. Cholesterol absorption was calculated using the following equation: % cholesterol absorption = ([^{14}C]/[^{3}H] dosing mixture – [^{14}C]/[^{3}H] feces)/([^{14}C]/[^{3}H] dosing mixture) × 100.

Lipid measurements in plasma

Plasma lipids were measured by a colorimetric assay with the Wako L-Type TG M kit and the Wako Cholesterol E kit. For fast protein liquid chromatography (FPLC), lipoprotein plasma samples (pools from 4-5 mice/group) were injected into a Superose 6 10/300 (GE Healthcare Life Sciences) FPLC column and fractions were collected for measurement of cholesterol by colorimetric assay.

Chylomicron isolation

To isolate chylomicrons, 0.5 mL of plasma were overlaid with 0.5 mL of saline. The samples were then centrifuged at 35,000 rpm in an Optima MAX-XP Ultracentrifuge for 60 min at 18°C. After centrifugation, the top layer was collected as the chylomicron fraction (~100 µL).

For the d4-cholesterol experiment, F/F and I-B/C KO mice were gavaged with 500 μg of d4-cholesterol in 100 μL of corn oil and injected with 10 mL/g Poloxamer-407. 3.5 h post-gavage, blood was harvested by cardiac puncture and centrifuged at 12,000*g* for 3 min. Plasma was collected. 700 μL of cold PBS+8.6 mM EDTA were transferred in ultracentrifuge tube and carefully underlaid with 300 μL of plasma. Samples were centrifuged in Beckman TLA-120.2
at 100,000 rpm at 10°C for 2 h. Chylomicrons were removed from the top of the tubes with a metal spatula and dissolved overnight at 4°C. 10 μL aliquots were used for lipid extraction and shotgun lipidomics.

Lipid measurement in liver

Livers were homogenized by dounce homogenizer in lysis buffer (10 mM Tris-HCl pH 7.4, 150 mM NaCl, 1 mM EDTA, protease inhibitors), and Folch method (*46*) was used to extract lipids from 0.5-1 mg liver protein. Protein content was measured by Bicinchoninic Acid Assay Protein Assay Kit (Pierce).

Lipid measurement in jejunum

Female mice were fasted for 4 h and gavaged with 2 μCi [^{14}C] cholesterol (Perkin Elmer) in 200 μl olive oil. 2 h later, mice were euthanized and small intestine was excised and flushed with 0.5 mM sodium taurocholate in PBS. Proximal jejunum (first 6 cm) was isolated, cut longitudinally, and minced with scissors. Then the minced tissue was homogenized in 1.6 mL lysis buffer (10 mM Tris-HCl pH 7.4, 150 mM NaCl, 1 mM EDTA, protease inhibitors) using a dounce homogenizer. The jejunum homogenates were collected into a glass tube and lipids were extracted by Bligh and Dier method (*47*). In brief, homogenizer was washed with 2 mL of methanol twice and the 4 mL were collected into a glass tube. 2 mL of chloroform were added to the tube, which was vortexed for 30 sec. Then 2 mL of chloroform and 2 mL 0.9% KCl were added to the tube, and the solution was vortexed for 15 sec. Samples were centrifuged at 2500 rpm for 10 min at room temperature. The lower layer was collected into a new glass tube, and the upper layer was subjected to an additional lipid extraction with 4 mL of chloroform. Samples were centrifuged at 2500 rpm for 10 min at room temperature, and the upper organic phase was collected into the same glass tube of the first extraction. The solvent was evaporated under N_2 and lipid film was resuspended in 100 mL of chloroform. Cholesterol and cholesterol esters were separated by thin-layer chromatography (TLC) on silica plates using the solvent system heptane: isopropyl ether: acetic acid (60: 40: 4). The silica plates were exposed on a phosphor screen (Cytiva/GE Healthcare Life Sciences), and the exposed screens were scanned with a bio-imaging analyzer (Typhoon Variable Mode Imager, GE, Piscataway, NJ) to quantify the incorporation of radioactivity in cholesterol and cholesterol esters.

Isolation of intestinal epithelial cells

To isolate intestinal epithelial cells, intestines were harvested and rapidly flushed with ice cold 1XPBS. Duodenum, jejnum and ileum were isolated with a ratio of 1:3:2, opened longitudinally, and sliced it in pieces of 5-6 cm. All the tissue pieces were quickly washed at room temperature in 50 mL of Buffer A (HBSS + 1% FCS) and gently shacked for 10 sec at room temperature for 5 times. Tissue pieces were washed in 20 mL of Buffer B Ca^{2+}/Mg^{2+} free HBSS + 2% glucose + 2% BSA, and incubated in 20 mL of pre-warmed enterocyte isolation buffer (Ca^{2+}/Mg^{2+} free HBSS + 0.5 mM DTT + 1.5 mM EDTA) at 37°C with shaking for 15 min. Supernatant were collected and centrifuged at 800 rpm 5 min at room temperature. Pelleted cells were incubated on ice. Intestinal pieces were re-incubated in 20 mL of fresh enterocyte isolation buffer and shacked at 37°C for 15 additional min. Supernatant from the second extraction was collected and transferred in the falcon tube containing cells from the first extraction. The cell suspension was centrifuged at 800 rpm 5 min at room temperature, and pellets were snap frozen in liquid nitrogen.

Protein isolation and immunoblot analysis

To prepare whole cellular lysates, enteroids from 4 wells were pooled and pelleted by quick centrifugation, and washed with 1 mL of PBS for 5 times. The pellets were resuspended in RIPA buffer supplemented with 1X protease and phosphatase inhibitor cocktails (Roche), by harsh pipetting and incubation on rotation at 4°C for 30 min. To prepare membrane-enriched lysates from intestine, duodenal or jejunal scrapings were homogenized with a dounce homogenizer in 500 mL-1 mL of lysis buffer (150 mM NaCl, 1.5 mM DTT, 50 mM Tris HCl pH 7.4, 1.25 mM EDTA, 0.1 mM PMSF) containing 1X protease and phosphatase inhibitor cocktails (Roche). Samples were quickly sonicated (3 pulses, 3 seconds on, 50%), and centrifuged at 4°C, 2000*g* for 10 min. Supernatants were collected and ultracentrifuged at 4°C, 100,000 *g* for 45 min. Pellets were resuspended in the lysis buffer (100-150 μL) using a Hamilton syringe. Protein content was determined by the Bicinchoninic Acid Assay Protein Assay Kit (Pierce), and an equal amount of protein (20 μg) per lane was loaded into NuPAGE 4-12% Bis-Tris gels (Invitrogen). Proteins were transferred to PVDF blotting membrane (Amersham Hybond, 10600023). Membranes were blocked for 1 hour

at room temperature with 5% milk in TBS + 0.1% Tween 20 (TBST), and incubated with primary antibodies as indicated in Table S1. Horseradish peroxidase-conjugated anti-mouse, anti-goat, and anti-rabbit IgG (Jackson) were used as secondary antibodies. The immune signal was visualized using the ECL kit (Amersham Biosciences).

RNA extraction and gene expression analyses

Total RNA was extracted using TRIzol (Invitrogen), quantified by NanoDrop (Thermofisher), and reverse transcribed. cDNA was quantified by real-time PCR using iTaq Universal SYBR Green Supermix (Bio-Rad) on a QuantStudio 6 Flex 384-well qPCR system (Applied Biosystems). Gene expression levels were determined by using a standard curve. Housekeeping gene *36b4* was used for normalization, and every sample was analyzed in duplicate. Primers used for real-time PCR are listed in table S2. For RNA sequencing, total RNA was extracted using TRIzol and the RNeasy Mini Kit with on-column DNase I digestion (Qiagen). Libraries were prepared using NEBNext Ultra II RNA Library Prep Kit for Illumina (New England Biolabs, Ipswich, MA, USA) and sequenced on Illumina HiSeq 4000 as paired-end 150 base pairs. Adapter and quality trimming of raw FASTQ files was performed using Trimmomatic (*48*). FastQC was used to analyze FASTQ files before and after trimming. Trimmed FASTQ files were aligned to GRCm38/mm10 using STAR (*49*). Aligned reads were visualized using Integrative Genomics Viewer (IGV). Gene counts were normalized and differential gene expression analysis was performed using DESeq2 (*50, 51*). The heatmap was created using the ClustVis web tool.

Lipidomic analysis

Intestinal scrapings (approximately 100 mg of proximal jejunum scrapings) were collected in a 2 mL homogenizer tube pre-loaded with 2.8 mm ceramic beads (Omni #19-628). PBS (0.75 mL) was added to the tube and the sample was homogenized in an Omni Bead Ruptor Elite (3 cycles of 10 sec at 5 m/s with a 10 second dwell time). Homogenate containing 2-6 mg of original tissue was transferred to a glass tube for extraction. A modified Bligh and Dyer extraction (*52*) was carried out on all samples. Prior to biphasic extraction, an internal standard mixture consisting of 70 lipid standards across 17 subclasses was added to each sample (AB Sciex 5040156, Avanti 330827, Avanti 330830, Avanti 330828, Avanti 791642). Following two successive extractions, pooled organic layers were dried down in a Thermo SpeedVac SPD300DDA using ramp setting 4 at 35 degrees C for 45 min with a total run time of 90 min. Lipid samples were resuspended in 1:1 methanol/dichloromethane with 10 mM ammonium acetate and transferred to robovials (Thermo 10800107) for analysis. Samples were analyzed on the Sciex 5500 with DMS device (Lipidyzer Platform) with an expanded targeted acquisition list consisting of 1450 lipid species across 17 subclasses (or the original acquisition list of 1100 lipids across 13 subclasses). Differential Mobility Device on Lipidyzer was tuned with EquiSPLASH LIPIDOMIX (Avanti 330731). Data analysis was performed on an in-house data analysis platform comparable to the Lipidyzer Workflow Manager (*53*). Quantitative values were normalized to mg of tissue, protein content, or plasma volume.

For cholesterol measurements, d7-cholesterol standard was added to each sample (Avanti 700041). Following extraction and lipidomic measurements, samples were derivatized with acetyl chloride (Fisher AA43262AD) and cholesterol was measured as acetyl esters as previously described (*54*).

In vivo back scattered electron (BSE) microscopy and NanoSIMS

2 WT and 2 Aster BC KO mice were fasted overnight, then refed for 2 h in order to synchronize digestive status. In the meantime, a mixture containing 40 mg [^{13}C] mixed fatty acids (Cambridge Isotopes Laboratories Inc. Andover, MA) and 4 mg [^{2}H] cholesterol per mouse was generated by combining 40 µL [^{13}C] mixed fatty acids (1 mg/µL) with sunflower oil (10 µL/mouse). Next, 4 mg [^{2}H] cholesterol (dissolved in pure ethanol) was mixed into the solution by pipetting. Ethanol was removed by evaporation under a constant stream of nitrogen for approximately 1 h. After 2 h of refeeding, mice were orally gavaged with the fatty acid/cholesterol mixture. 2 h later, mice were anesthetized, then the abdominal cavity was opened and intestines were placed directly into fixative (2.5% glutaraldehyde, 2% paraformaldehyde, 2.1% sucrose, 0.1 M sodium cacodylate), then small, ring-shaped slices were cut from the appropriate regions of the small intestine. Intestine slices were then fixed in the same fixative at 4ºC overnight. The following day, the samples were washed 5x5 min in cold 0.1 M sodium cacodylate and then postfixed with reduced osmium (2% OsO_4, 1.5% potassium ferricyanide, 0.1 M sodium cacodylate) for 1 h. Next, samples were washed 5 x 5 min in cold H_2O then treated with 1% thiocarbohydrazide for 20 min at room temperature. Samples were then rinsed with H_2O 5x5 min and stained again with osmium (2%OsO_4 in H_2O) for 30 min. After another round of H_2O washes, the tissue was stained with 1% uranyl acetate (SPI Chem.) at 4ºC overnight. Tissues were dehydrated by incubating in a graded series of ethanol solutions (30%, 50%, 70%, 85%, 95%, 100%X3) for 8 min each. T hen tissues were infiltrated with 33% (in acetone) EMbed812 for 1 h, 66% overnight, then 100% for 4 h. Individual tissue pieces were then embedded in a flat mold and polymerized in a

vacuum oven for 48 h. Resin blocks were then trimmed and 500 nm sections were collected onto small silicon wafers using a Leica UC6 ultramicrotome and a Diatome diamond knife. For backscattered electron microscopy (BSEM): Wafers were mounted onto SEM stubs with double-sided carbon tape and imaged using a Zeiss Supra 40VP SEM equipped with a backscattered electron detector. Accelerating voltage was set to 13KeV and working distance at approx. 5 mm. BSEM was performed at the Electron Imaging Center for Nanomachines which is a part of the California NanoSystems Institute at UCLA. For correlative backscattered electron microscopy and NanoSIMS imaging, regions of interest were imaged using an FEI Verios XHR SEM with the 2-kV electron beam of 0.2-nA beam current and a backscattered electron detector (CBS). Mosaics of images were collected with the Maps 2.0 software and were stitched with Grid/Collection stitching in Image J (*55*). The same samples were coated with 5 nm platinum on the surface and transferred into a NanoSIMS 50L (CAMECA, France) for NanoSIMS analysis. A $^{133}Cs+$ primary ion beam of ~1 nA beam current was used for the implantation of cesium onto the sample surface (aperture D1 = 1) to reach a total ion dose of $\sim 1\times10^{17}$ ions/cm^2. $^1H–$, $^2H–$, $^{12}C–$, and $^{13}C–$ secondary ion signals were collected to visualize and quantify the distributions of [^{2}H]cholesterol and ^{13}C-labelled mixed fatty acids. Images were obtained using aperture D1 = 2 with a current of ~3 pA, a dwell time of 3.0 ms/pixel, and a raster size of 30 µm × 30 µm. Mosaics of NanoSIMS images were obtained on the same areas that were mapped with backscattered electron imaging.

Isolation of murine crypts

Murine crypts were isolated from the jejunums of 8- to 12-week-old 3×HA Aster-B, WT, and Aster BC KO mice as previously described (*56*). Animals were euthanized with isoflurane, and the jejunum was harvested and flushed with ice-cold PBS. The intestine was inverted to expose the villous surface and submerged in 30 ml 2.5 mM EDTA/PBS on a rocker at 4°C for 30 min. The supernatant was discarded and replaced with 15 mL PBS. The tube was then vortexed in 3-second pulses 10 times, to release crypts from the tissue. Leaving the tissue behind, the mixture was poured into a new 15 mL conical tube and settled on ice for 5 min to allow unwanted cells and connective tissue to fall to the bottom. The supernatant containing the crypt fraction was filtered through a 70 mm cell strainer into a new 15 ml conical tube. The crypts were centrifuged at 100*g* for 2 min. The pellet was washed with 5 mL PBS and centrifuged at 100*g* for 2 min. The supernatant was removed and the pellet was suspended in Matrigel to a final concentration of 200 crypts per 25 µl. 25 µl of crypt/Matrigel suspension was plated into the wells of a 48-well plate and placed in a 37°C, 5% CO_2 incubator for 20 min to polymerize. 250 µl of growth medium was added to each well. Growth medium contained the following: 50% Advanced DMEM/F12 (Gibco 12634-010), 50% L-WRN conditioned medium (*56*), 2 mM GlutaMAX, 10 mM HEPES, 100 U/ml penicillin, 100 µg/ml streptomycin, 1X N2 supplement (Gibco 17502-048), 1X B27 supplement (Gibco 17504-044), 50 ng/ml EGF (Peprotech 315-09), 1 mM N-acetylcysteine (Sigma A9165-5G), 2.5 µg/ml fungizone, and 200 µg/ml normocin. 10 µM Y-27632 (Sigma Y0503) was added for the first few days after extraction and after splitting.

Culture and expansion of murine enteroids

Enteroids were passaged every 7-10 days. After removing the medium, the Matrigel was broken with ice-cold PBS to release the enteroids. The solution was pelleted and washed 2 additional times with PBS. After the final wash, the pellet was suspended in 200 µl of PBS and the enteroids were broken by pipetting 5-10 times. The broken enteroids were centrifuged and the supernatant was aspirated. 10 µl of growth medium was added to the pellet before resuspending in Matrigel. 25 µl of the enteroid/Matrigel suspension was plated into the wells of a 48-well plate, and growth medium was added to the wells after polymerization. Enteroids passaged more than 4 times, but less than 30 times, were used for the experiments. Prior to use, enteroids were differentiated for 5 days in murine differentiation medium, containing Advanced DMEM/F12, 2 mM GlutaMAX, 10 mM HEPES, 100 U/ml penicillin, 100 µg/ml streptomycin, 1X N2 supplement, 1X B27 supplement, 50 ng/ml EGF, 50 ng/ml noggin (Peprotech 250-38), 50 ng/ml r-Spondin1 (R and D 3474-RS), 10 µM Y-27632, 2.5 µg/ml fungizone, and 200 µg/ml normocin.

Culture of apical-out murine enteroids

Basolateral-out enteroids were everted to generate apical-out enteroids, as previously described (*37*). The Matrigel of young basolateral-out enteroids (day 3-5) was broken with ice cold PBS and transferred into a microcentrifuge tube. The enteroids were centrifuged at 2,000 g for 5 seconds and the supernatant was aspirated. To ensure adequate removal of Matrigel, the pellet was resuspended in cell recovery solution (Corning 354253) and incubated at 4°C for 20 min. The enteroids were pelleted and resuspended in 1 ml of 5 mM EDTA/PBS solution. The solution was transferred to a 15 ml conical tube containing 10-12 ml 5 mM EDTA/PBS and incubated on a rotating platform at 4°C for 1 h. The tubes were centrifuged at 300*g* for 3 min and the ETDA/PBS solution was aspirated.

The pellet containing the enteroids was washed with 5 ml PBS and centrifuged at 300*g* for 3 min. The pellet was resuspended in enteroid growth medium with 10 μM Y-27632 and plated in ultra-low attachment plates. After 1-2 days, the medium was exchanged for murine differentiation medium with 10 μM Y-27632 and the enteroids were allowed to differentiate for 5 days. The medium was changed every 2-3 days.

Culture of basolateral-out human enteroids

De-identified human enteroids were provided as a gift b the laboratory of Dr. Martin Martin. The enteroids were expanded and passaged every 7-10 days, using the same method as for murine enteroids. Human enteroids were cultured in growth medium containing 50% Advanced DMEM/F12 (Gibco 12634-010), 50% L-WRN conditioned medium (*57*), 2 mM GlutaMAX, 10 mM HEPES, 100 U/ml penicillin, 100 μg/ml streptomycin, 1X N2 supplement, 1X B27 supplement, 50 ng/ml EGF, 1 mM N-acetylcysteine, 500 nM A83-01 (Tocris 909910-43-6), 10 μM SB202190 (Sigma S7067), 2.5 μg/ml fungizone, and 200 μg/ml normocin. 10 μM Y-27632 was added for the first few days after passaging the enteroids. Enteroids were differentiated for 5 days prior to use for experiments. Human differentiation medium contained Advanced DMEM/F12, 2 mM GlutaMAX, 10 mM HEPES, 100 U/ml penicillin, 100 μg/ml streptomycin, 1X N2 supplement, 1X B27 supplement, 50 ng/ml EGF, 50 ng/ml noggin, 50 ng/ml r-Spondin, 500 nM A83-01, 10 μM Y-27632, 2.5 μg/ml fungizone, and 200 μg/ml normocin.

Culture of human intestinal epithelial cells on transwell membranes for gene expression

Human intestinal epithelial cells (IECs) were derived from basolateral-out human jejunal enteroids to culture IECs as a monolayer on transwell membranes. Basolateral-out enteroids were extracted from Matrigel with PBS and incubated in cell recovery solution for 20 min at 4°C. The enteroids were pelleted and the supernatant was removed. The pellet was resuspended in TrypLE for 10 min at 37°C to obtain single cells. Medium was added to stop the reaction and the mixture was centrifuged to pellet the cells. The cells were resuspended in growth medium containing 50% Advanced DMEM/F12 (Gibco 12634-010), 50% L-WRN conditioned medium, 2 mM GlutaMAX, 10 mM HEPES, 100 U/ml penicillin, 100 μg/ml streptomycin, 1X N2 supplement, 1X B27 supplement, 50 ng/ml EGF, 1 mM N-acetylcysteine, 500 nM A83-01, 10 μM SB202190, 10 μM Y-27632, 2.5 μg/ml fungizone, and 200 μg/ml normocin. 150,000 cells were plated per transwell. On day 2, the medium was changed to human differentiation medium and changed every other day. After 5 days of differentiation, cells were deprived of cholesterol by overnight incubation with 1 mM Ro 48-8071 (Cayman Chemical, 10006415) and 50 mM mevalonate. Of note, human differentiation medium contains no cholesterol. After 16 h, cells were pre-treated with vehicle or 5 mM AI-3d for 2.5 h. The monolayer was then loaded with mixed micelles containing 6 mM oleic acid (Cayman Chemical, 90260), 0.5 mM cholesterol (Sigma, C8667), 2 mM 2-palmitoylglycerol (Cayman Chemical, 17882), 2 mM Lyso-PC (Avanti, 845875C), 40 mM sodium taurocholate (Sigma, 86339), 1 μM Ro 48-8071, and 50 μM mevalonate, in the presence of vehicle or 5 μM AI-3d. After 4 h, cells were processed for RNA extraction.

Immunofluorescence

HA tagged Aster-B enteroids grown basolateral-out were differentiated for 5 days and pre-treated with 1 μM Ro 48-8071 and 50 μM mevalonate for 1.5 h, then incubated with vehicle or 150 μM MbCD-cholesterol for 2 h. The enteroids were extracted from Matrigel using ice cold PBS and incubated in cell recovery solution for 1 h at 4°C. The enteroids were washed with PBS, then fixed using 4% paraformaldehyde for 20 min at room temperature. The enteroids were allowed to settle to the bottom, and the fixative was aspirated. Permeabilization was performed with 0.3% Triton for 15 min at room temperature. The enteroids were blocked with 10% goat serum in PBS for 1 h at room temperature and incubated in primary antibody (Anti-HA C29F4, 1:1000, CST 3724S) overnight at 4°C. The following day, the enteroids were washed with 2X PBS for 2 min 3 times and incubated with secondary antibody (anti-rabbit AF594, 1:1000, CST 8889S) for 60-90 min at room temperature. The enteroids were washed again with 2X PBS for 2 min 3 times, and then transferred to a glass slide. ProLong Diamond Antifade Mountant with DAPI (Invitrogen P36962) was applied to the slide prior to placement of the cover slip. The same protocol was applied to apical-out enteroids, but they were not previously incubated in cell recovery solution. Imaging was performed on a Zeiss LSM 900 confocal microscope equipped with 405 nm, 488 nm, 561 nm, and 640 nm laser lines using a Plan-Apochromat 20x/0.8 or Plan-Apochromat 40x/1.2 objective and Airyscan 2 GaAsP-PMT detector. Identical laser intensity settings were applied to each experimental sample set, and Z-stacks were performed to acquire equivalent section thicknesses. After acquisition, a maximum intensity projection of the Z-stack was applied using ZEN Blue 3.0 software. HA tagged Aster-B enteroids grown apical-out were processed in a similar fashion with the exception of a longer cholesterol depletion period, with 1 μM Ro 48-8071 and 50 μM mevalonate for 16 h overnight. On the day of the experiment, enteroids were pre-treated with vehicle or 0.025 mM ezetimibe for 2 h before treatment with

mixed micelles containing 6 mM oleic acid, 0.5 mM cholesterol, 2 mM 2-palmitoylglycerol, 2 mM Lyso-PC, 40 mM sodium taurocholate, 1 mM Ro 48-8071, and 50 mM mevalonate, in the presence of vehicle or 0.025 mM ezetimibe for an additional 2 h. Enteroids underwent fixation and staining as outlined above.

Purification and fluorophore conjugation of ALOD4

pALOD4 (*35*) was purified as previously described (*58*). Briefly, plasmid encoding ALOD4 was expressed in BL21 (DE3) pLysS *E. coli* (Invitrogen). Cell pellets were lysed by sonication in lysis buffer with 50 mM NaH_2PO_4, pH 7.0, 300 mM NaCl, 1 mg/ml lysozyme, 1 mM DTT, 2 mM phenylmethylsulfonyl fluoride (PMSF), and protease inhibitor cocktail tablet (Themo Scientific). Protein was bound to HisPur Ni-NTA Agarose resin (Thermo Scientific), washed twice with 50 mM imidazole, eluted with 300 mM imidazole, and subjected to size exclusion chromatography on Superdex 200. Fractions containing ALOD4 were concentrated to 1 mg/ml and stored at -80C with glycerol. ALOD4 was conjugated to Alexa 488 C5 maleimide (Thermo Fisher) followed by affinity chromatography using HisPur Ni-NTA Agarose resin as above. Samples were dialyzed to remove imidazole prior to determination of labeling efficiency on Nanodrop (Thermo Fisher).

ALOD4 staining in enteroids

Human and murine basolateral-out enteroids were differentiated for 5 days. Enteroids were deprived of cholesterol in differentiation medium containing 1 μM Ro 48-8071 and 50 μM mevalonate for 16 h. Murine WT and BC KO enteroids were treated with vehicle or 150 μM MbCD-cholesterol for 1 h. For the AI3d experiment, murine and human WT enteroids were pre-treated with vehicle or 5 μM AI-3d + 1 μM Ro 48-8071 and 50 μM mevalonate for 5 h, and then treated with vehicle or 150 μM MbCD-cholesterol for 1 h in presence or absence of 5 μM AI3d.

Enteroids in Matrigel were washed with cold dPBS (+ Ca, + Mg) and 0.2% bovine serum albumin (BSA), 3 times. The enteroids were then collected in 400 μl of cell recovery solution with ALOD4 at a concentration of 20 μg/ml and remained in solution for 1 hour at 4°C. After incubation, the enteroids were washed with dPBS (+ Ca, + Mg) and 0.2% BSA 4 times, 2 min each prior to fixation with 4% paraformaldehyde at room temperature for 15 min. The enteroids were again washed with dPBS (+ Ca, + Mg) and 0.2% BSA 4 times, 5 min each. The sample was mounted on glass slides with ProLong Diamond Antifade Mountant with DAPI and secured with a cover slip. Imaging was performed on a Zeiss LSM 900 confocal microscope using 405 nm and 488 nm laser lines for excitation. Images were acquired using a Plan-Apochromat 20x/0.8 or Plan-Apochromat 40x/1.2 objective and Airyscan 2 GaAsP-PMT detector. Identical laser intensity settings were applied to each experimental sample set and Z-stacks were performed to acquire equivalent section thicknesses for comparison across treatments. After acquisition, a maximum intensity projection of the Z-stack was applied using ZEN Blue 3.0 software.

Caco-2 cells

Caco-2 (HTB-37, ATCC) cells were seeded in 12-well transwell plate (Corning) at a density of 3×10^5 cells/cm^2 (approximately 350,000 cells/well) and cultured in DMEM + 10% fetal bovine serum (FBS) with 1% PenStrep (Gibco), on both apical and basolateral side. Cells were cultured in transwell up to 20 days, changing medium every other day, and transepithelial electrical resistance (TEER) was measured at day 7, day 14, and day 20. Cells with a TEER measurement around 1200 were considered ready for experiments. For AI-3d treatment, cells at day 16 of differentiation were cholesterol-deprived by overnight incubation with DMEM containing 1% lipoprotein-deficient serum (LPDS), 1 mM Ro 48-8071 (Cayman Chemical, 10006415), and 50 mM mevalonate. After 16 h, cells were pretreated with vehicle or 5 mM AI-3d in DMEM with 1% LPDS, 1 mM Ro 48-8071, and 50 mM mevalonate for 2.5 h. Caco-2 cells were then loaded with DMEM supplemented with mixed micelles containing 6 mM oleic acid (Cayman Chemical, 90260), 0.5 mM cholesterol (Sigma, C8667), 2 mM 2-palmitoylglycerol (Cayman Chemical, 17882), 2 mM Lyso-PC (Avanti, 845875C), 40 mM sodium taurocholate (Sigma, 86339), 1 μM Ro 48-8071, and 50 μM mevalonate, in the presence of vehicle or 5 μM AI-3d. After 3 h, cells were processed for RNA extraction.

McArdle

McArdle RH7777 rat hepatoma cell line (CRL-1601, ATCC) cells were maintained in DMEM containing 100 units/ml penicillin and 100 μg/ml streptomycin sulfate supplemented with 10% FBS. For cholesterol depletion, cells were incubated with depleting medium (DMEM containing 5% LPDS, 10 μM compactin, 50 μM mevalonate, and 1.5% MbCD) for 1 h. For cholesterol replenishment, cells were incubated in DMEM containing 5% LPDS, 10 μM compactin, 50 μM mevalonate, and 100 μM MbCD-cholesterol for 2 h. Stable cell lines expressing NPC1L1-EGFP and HA-Aster-B were selected with 1 μg/mL puromycin.

Protein Expression and Purification

Protein expression and purification of mouse Aster-$C_{296-517}$ was undertaken as described previously for Aster-A (*25*). Excess EZ was added to partially purified Aster-C (molar ratio 1:5, protein: ligand) from a 10 mg/ml stock solution dissolved in ethanol before loading the complex on a Superdex S-200 column. The fractions containing the Aster-C: EZ complex were concentrated to 6 mg/ml and used for the crystallization experiments. Site-directed mutagenesis was performed to generate the following mouse Aster-$A_{334-562}$ mutants: AsterA_L400A_F405I, AsterA_L400A, and AsterA_F405I, and the following mouse Aster-$C_{296-517}$ mutants: AsterC_A357L_I362F, AsterC_A357L, and AsterC_I362F. The resulting inserts were cloned and purified as described previously (*36*), without adding any compound to the protein samples. Instead, 10 % of glycerol was added to the gel filtration buffer, and the resulting samples were used for circular dichroism experiments.

Crystallization and X-Ray Structure Determination

Crystals of the Aster-$C_{296-517}$ in complex with EZ ligand were obtained using sitting drop vapor diffusion at room temperature. Crystals were grown using 0.2 M sodium chloride, 0.1 M MES pH 6.5, and 10% PEG 4000 (condition B4, PROPLEX, Molecular Dimensions). The crystals were cryo-protected with 30% glycerol, 0.2 M sodium chloride, 0.1 M MES pH 6.5, and 10% PEG 4000. Data were collected to 1.6 Å on the I24 beamline at Diamond Light Source, UK. Data were processed using XDS (within Xia2) and Pointless/Aimless (within CCP4) (*59-61*). The structure was solved using molecular replacement using Phaser (within CCP4) (*62*) and the Aster-A structure (PDB ID code 6GQF) as a template (*25*). Model fitting and refinement were performed using Coot, ArpWarp, Refmac (within CCP4), and Phenix (*63-66*). The structure has been submitted to the PDB database, PDB ID code 8AXW.

Circular Dichroism

Thermal unfolding of mouse Aster-$A_{334-562}$ wild-type and mutants, Aster-$B_{303-533}$, and Aster-$C_{296-517}$ wild-type and mutants was monitored by circular dichroism (CD) spectroscopy over a range of 200 to 250 nm, using a Chirascan Spectrometer (Applied Photophysics) equipped with a temperature controller (Quantum Northwest TC125). CD spectra were measured from samples in 1-mm-path-length quartz cuvettes, using a scanning speed of 100 nm/min, a spectral bandwidth of 1 nm, and a response time of 1 s. The thermal denaturation or unfolding profile of the proteins was characterized by measuring the ellipticity changes at 222 nm induced by a temperature increase from 20 to 90 ºC with steps of 1 degree. Samples of 1 mg/ml protein, apo or in complex with 25-HC, EZ or U18666A, were used. Melting temperature values were obtained by analyzing the data using GraphPad Prism and a nonlinear regression analysis.

Supplementary Figures

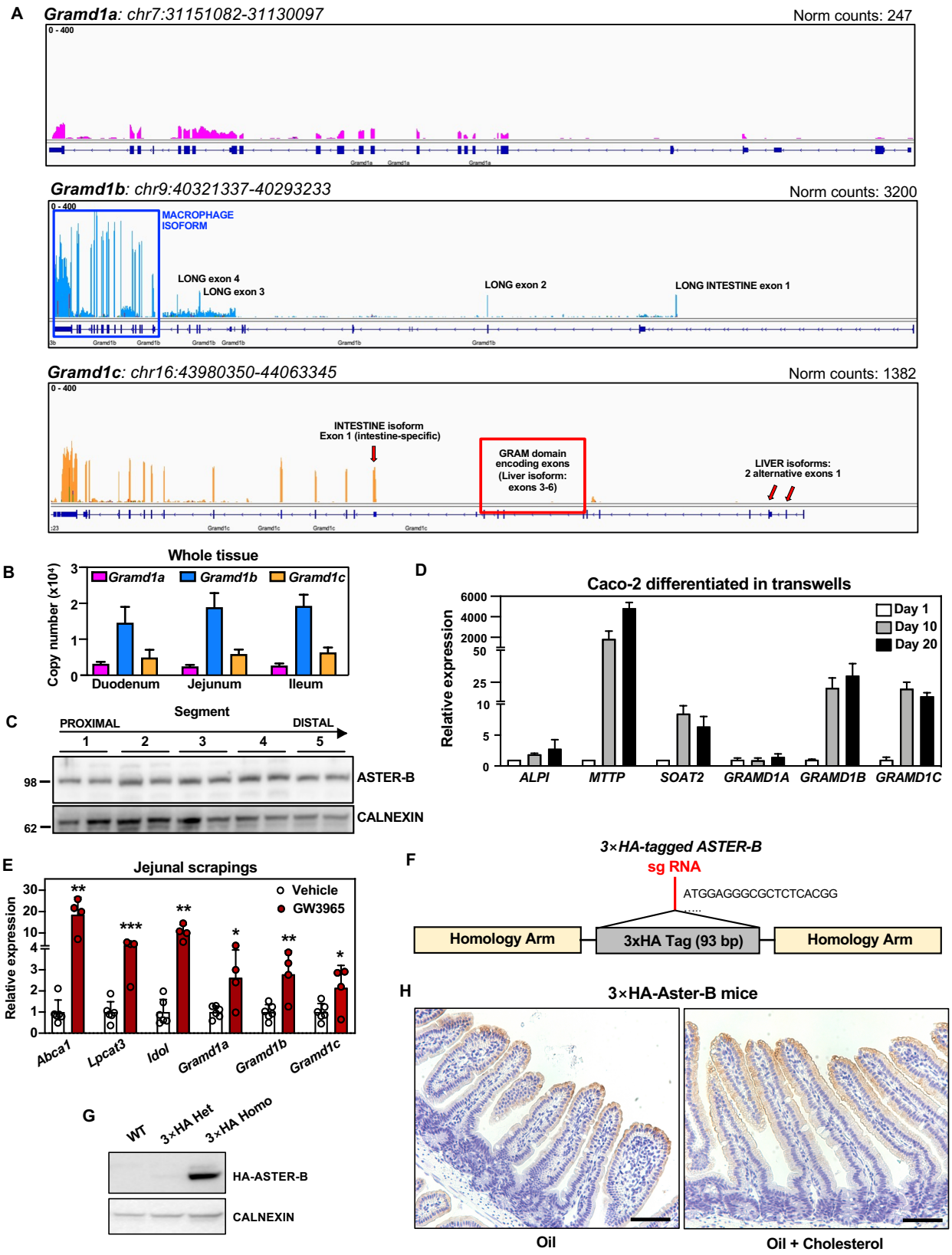

Ferrari et al, Fig. S1

Fig. S1. Expression and regulation of Aster variants in small intestine.

(**A**) RNA sequencing tracks of *Gramd1a*, *Gramd1b*, and *Gramd1c* from proximal jejunum of WT mice. (**B**) Quantification of *Gramd1a*, *Gramd1b*, and *Gramd1c* transcripts in intestinal epithelial cells (IECs) isolated from duodenum, jejunum and ileum of C57BL6/J male mice (*n = 5*). (**C**) Western blot analysis of expression of ASTER-B along the small intestine in C57BL6/J male mice (*n = 2*). (**D**) Gene expression of differentiation markers and of *GRAMD1A*, *GRAMD1B*, and *GRAMD1C* in Caco-2 cells that had been differentiated on transwell plates. (**E**) Gene expression of LXR targets and *Gramd1a*, *Gramd1b*, and *Gramd1c* in jejunum scrapings from mice treated with vehicle (*n = 6*) or the LXR ligand GW3965 (*n = 4*) for 8 h. (**F**) Generation of 3×HA-Aster-B mice by CRISPR/Cas9 based strategy. (**G**) Detection of 3×HA-Aster-B in small intestine by western blot. (**H**) Immunohistochemistry of HA-Aster-B in small intestines from 3×HA-Aster-B mice, showing higher expression in the villi. Scale bar is 50 μm. Data are expressed as mean ± SEM. Statistical analysis: unpaired *t* test, *p < 0.05, **p < 0.01, ***p < 0.001.

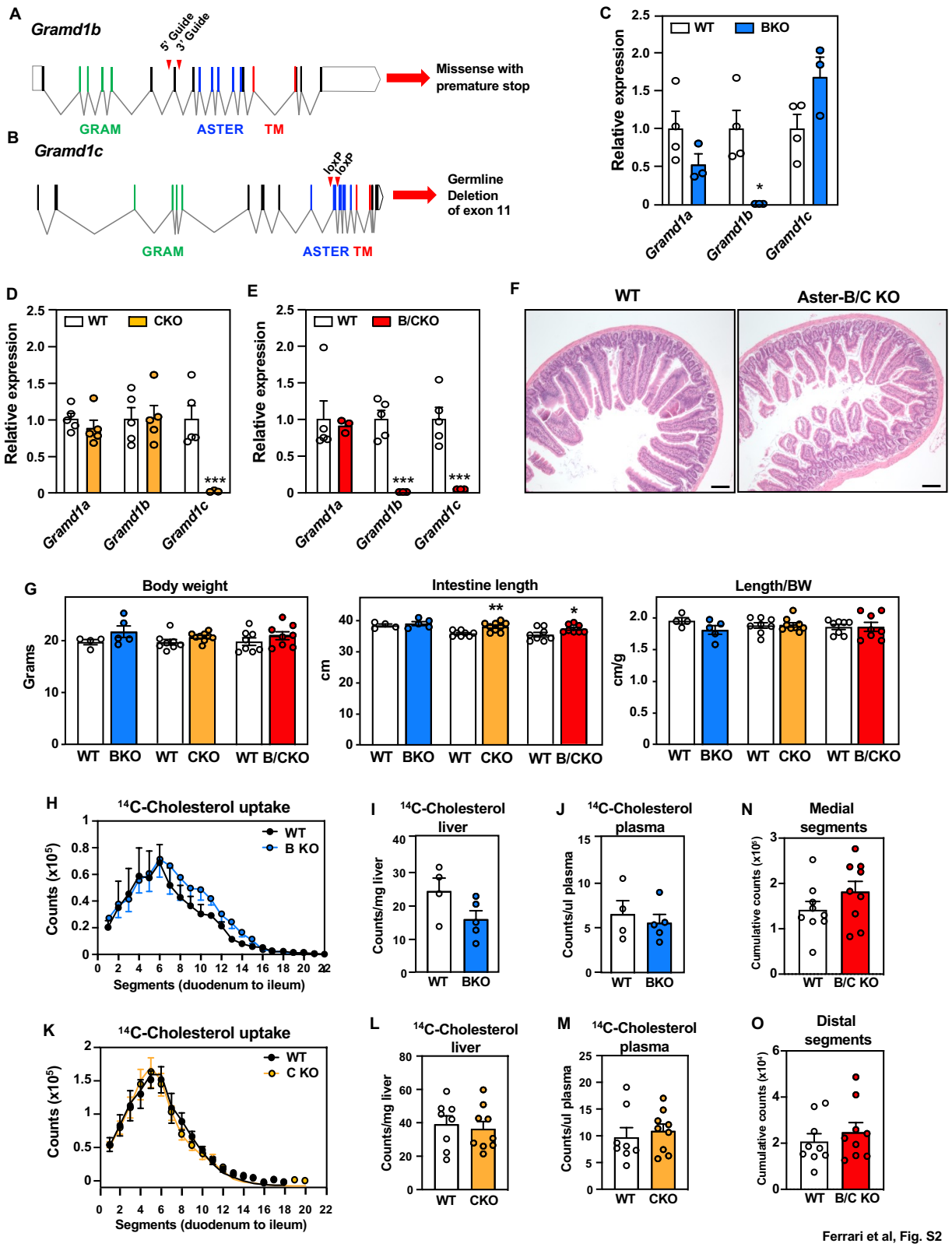

Ferrari et al, Fig. S2

Fig. S2. Preserved cholesterol absorption in global Aster-B and Aster-C single KO mice. (**A**) Generation of Aster-B global KO (BKO) mice. (**B**) Generation of Aster-C global KO (CKO) mice. (**C**) Deletion of Aster-B in single KO confirmed by qPCR (*n = 4-3/group*) (**D**). Deletion of Aster-C in single KO confirmed by qPCR (*n = 5/group*). (**E**) Deletion of Aster-B and Aster-C in double KO confirmed by quantitative PCR (*n = 5-3*/group). (**F**) Hematoxylin and eosin staining of proximal jejunum of WT and Aster-B/C global knockout (B/C KO) mice. Scale bar is 200 μm. (**G**) Body weight, intestinal length and intestinal length normalized on body weight of BKO, CKO, and B/C KO mice compared to littermates WT (*n = 4–9*/group). (**H**) Distribution of radioactivity in intestinal segments of female WT (*n = 4*) and BKO (*n = 5*) mice after an oral challenge of olive oil containing [^{14}C]cholesterol for 2 h. (**I**) Radioactivity in liver of mice described in I. (**J**) Radioactivity in plasma of mice described in H. (**K**) Distribution of radioactivity in intestinal segments of female WT (*n = 8*) and CKO (*n = 9*) mice after an oral challenge of olive oil containing [^{14}C]cholesterol for 2 h. (**L**) Radioactivity in liver of mice described in L. (**M**) Radioactivity in plasma of mice described in L. (**N**) Cumulative radioactive counts in the medial intestine (medial jejunum + distal jejunum) of mice described in Fig. 1D. (**O**) Cumulative radioactive counts in the distal intestine (ileum) of mice described in Fig. 1D. Data are expressed as mean ± SEM. Statistical analysis: unpaired *t* test, *p < 0.05, **p < 0.01, ***p < 0.001.

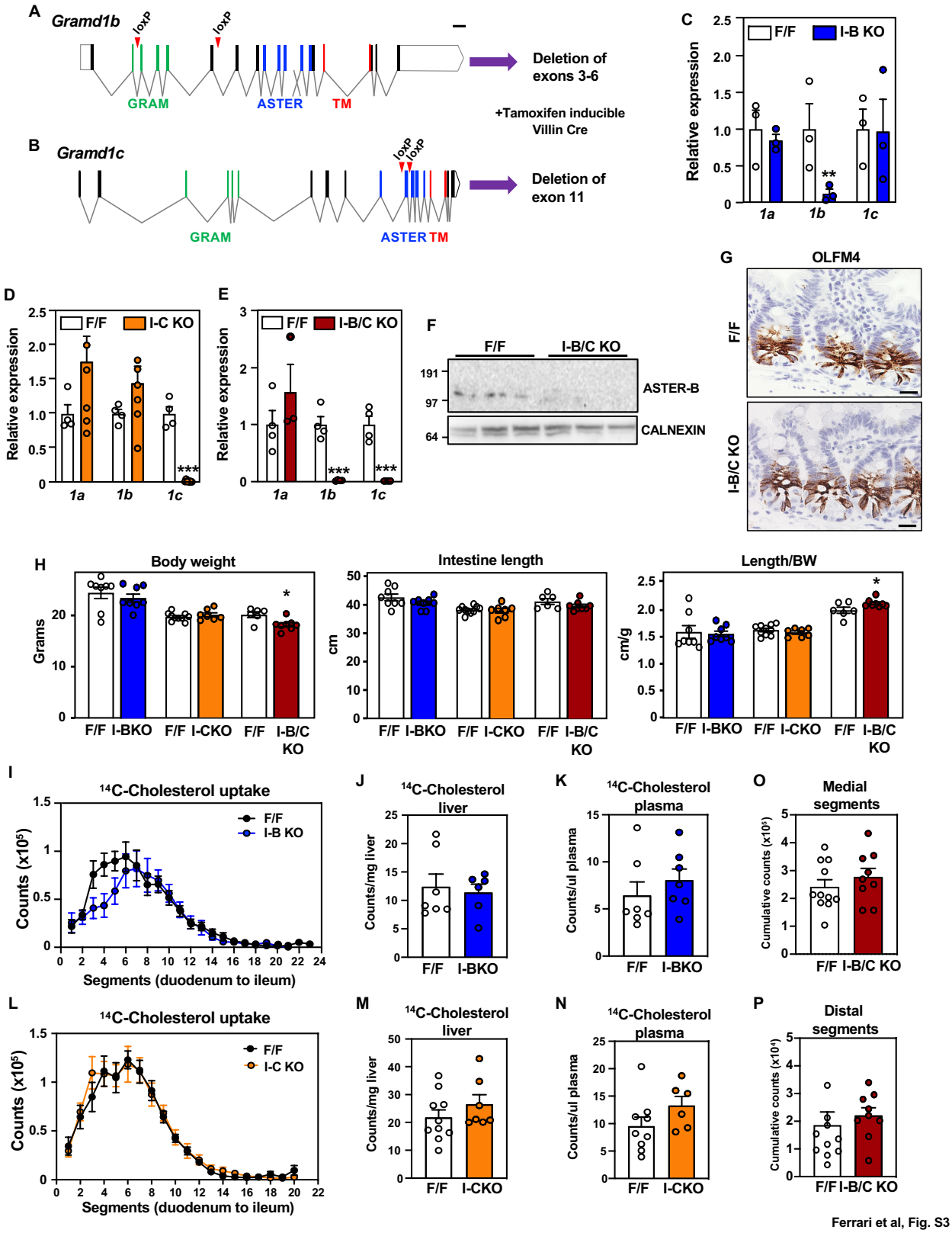

Ferrari et al, Fig. S3

Fig. S3. Preserved cholesterol absorption in inducible Aster-B and Aster-C single-KO mice. (**A**) Generation of intestinal tamoxifen-inducible Aster-B conditional KO (I-BKO) mice. (**B**) Generation of intestinal tamoxifen-inducible Aster-C conditional KO (I-CKO) mice. (**C**) Deletion of Aster-B in single conditional KO mice confirmed by qPCR (*n = 3/group*). (**D**) Deletion of Aster-C in single conditional KO mice confirmed by qPCR (*n = 4-5/group*). (**E**) Deletion of Aster-B and Aster-C in double conditional KO mice confirmed by quantitative PCR (*n = 4–3*/group). (**F**) Western blot analysis confirmed deletion of Aster-B in I-B/C KO mice (n = 3/group). (**G**) Immunohistochemistry of OLFM4 in jejunum of F/F and I-B/C KO. Scale bar is 20 μm. (**H**) Body weight and intestinal length of I-BKO, I-CKO, and I-B/C KO mice compared to F/F littermates (*n = 6–10*/group). (**I**) Distribution of [^{14}C]cholesterol radioactivity in intestinal segments of male F/F (*n = 7)* and I-BKO (*n = 6*) mice after an oral challenge of olive oil containing [^{14}C]cholesterol for 2 h. (**J**) Radioactivity in liver of mice described in I. (**K**) Radioactivity in plasma of mice described in I. (**L**) Distribution of radioactivity in intestinal segments of female F/F (*n = 10*) and I-CKO (*n = 7*) mice after an oral challenge of olive oil containing [^{14}C]cholesterol for 2 h. (**M**) Radioactivity in liver of mice described in K. (**N**) Radioactivity in plasma of mice described in L. (**O**) Cumulative radioactive counts in the medial intestine (medial jejunum + distal jejunum) of mice described in Fig. 1G. (**P**) Cumulative radioactive counts in the distal intestine (ileum) of mice described in Fig. 1G. Data are expressed as mean ± SEM. Statistical analysis: unpaired *t* test; *p < 0.05, **p < 0.01, ***p < 0.001.

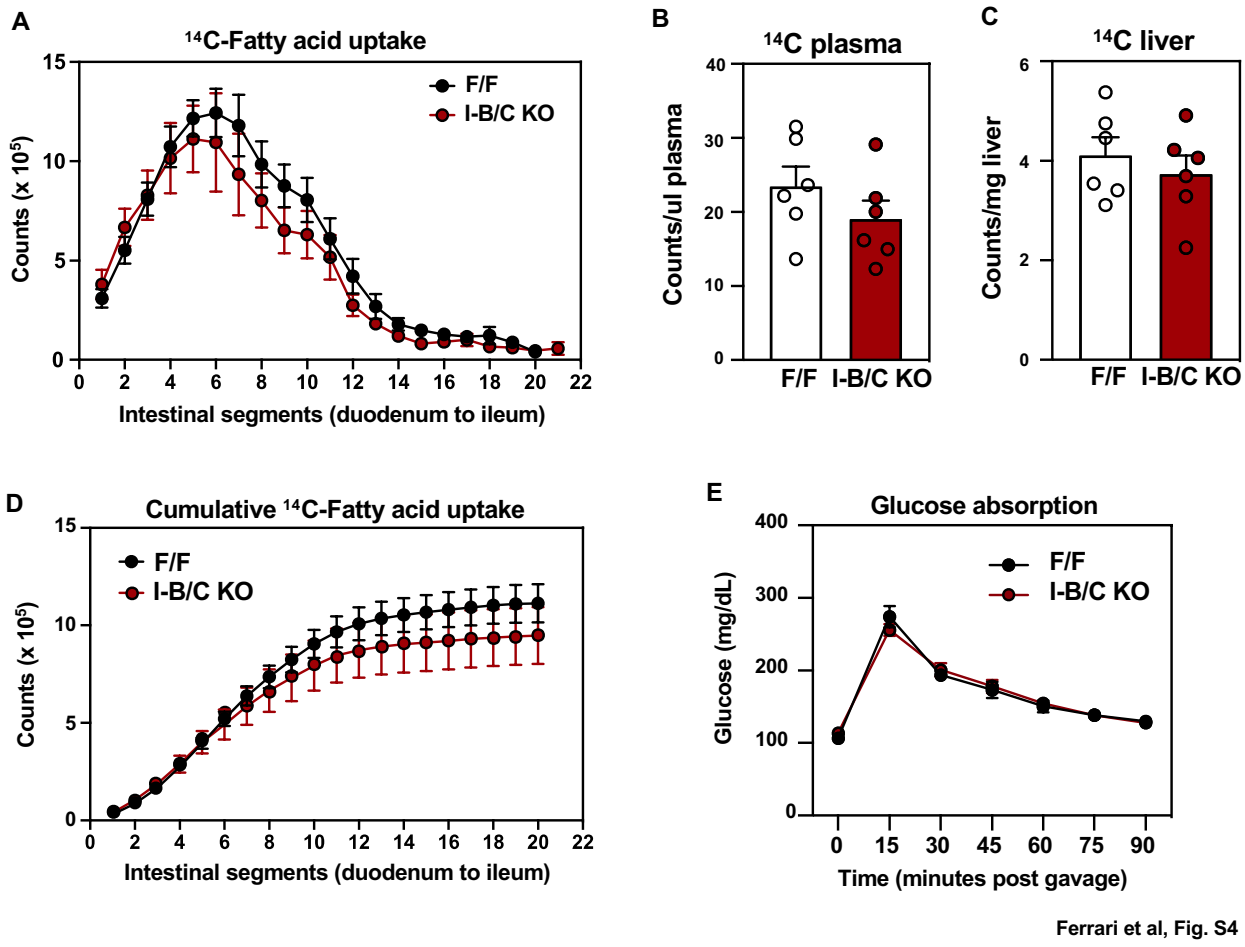

Fig. S4. Fatty acid absorption is intact in intestine-inducible Aster-B/C KO mice.
(**A**) Distribution of radioactivity in intestinal segments of female F/F and I-B/C KO mice after an oral challenge of olive oil containing [^{14}C]triolein for 2 h (*n* = *6*/group). (**B**) Radioactivity in plasma of mice described in A. (**C**) Radioactivity in liver of mice described in A. (**D**) Cumulative radioactivity in intestinal segments of mice described in (A). (**E**) Glucose uptake, measured as plasma glucose appearance in female F/F and I-B/C KO mice after oral gavage of 2 mg/kg glucose. Data are expressed as mean ± SEM. Statistical analysis: for panels A, D, E, 2-way ANOVA with Tukey's multiple comparisons test; for panels B, C, unpaired *t* test; *p < 0.05, **p < 0.01, ***p < 0.001.

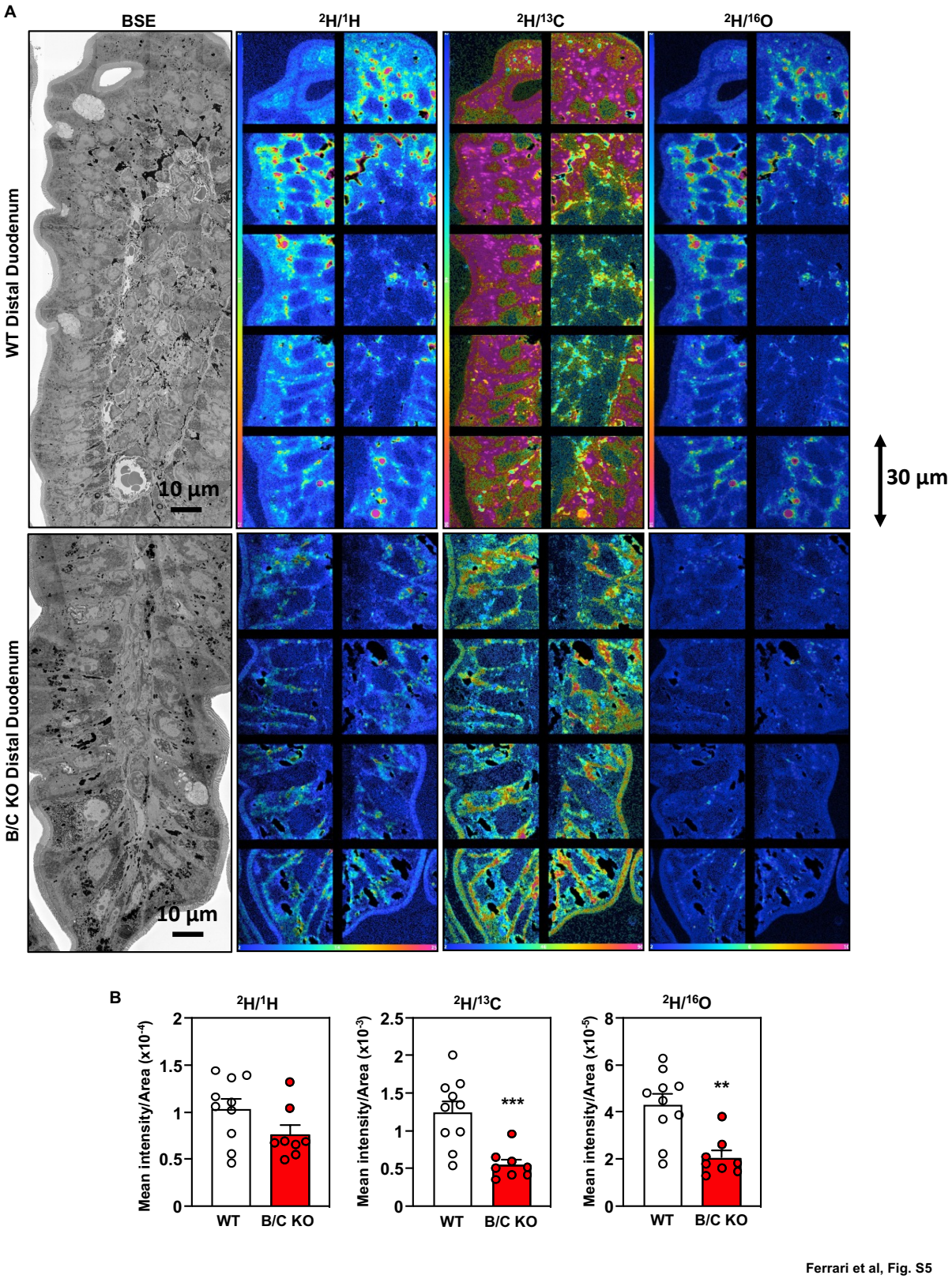

Ferrari et al, Fig. S5

Fig. S5. Intestinal deletion of Asters reduces accumulation of dietary derived cholesterol in distal duodenum.

(**A**) Backscattered electron images and NanoSIMS images of the distal duodenum from WT and B/C KO mice after having been given, by gastric gavage, a mixture of [^{2}H]cholesterol and [^{13}C]mixed fatty acids. (**B**) Quantification of $^{2}H^{-}$ secondary ions from the intestinal villus, relative to $^{1}H^{-}$, $^{13}C^{-}$, and $^{16}O^{-}$ secondary ions. Data are expressed as mean ± SEM. Statistical analysis: unpaired *t* test; *p < 0.05, ***p < 0.001, ****p < 0.0001.

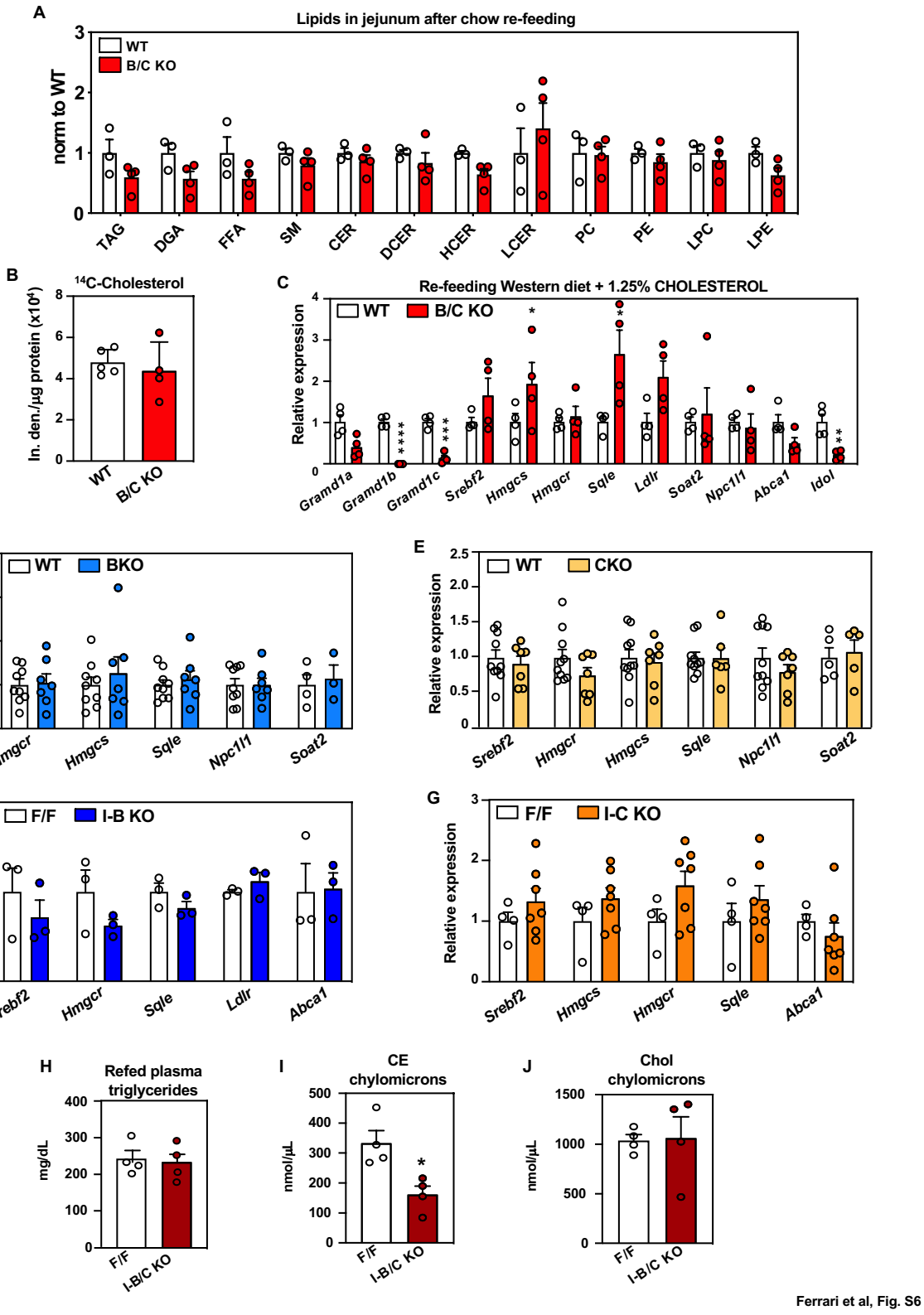

Ferrari et al, Fig. S6

Fig. S6. Characterization of phenotypical effect of Aster deletion on intestinal cholesterol metabolism.

(**A**) Lipidomic analysis in proximal jejunum of WT (*n = 3*) and B/C KO (*n = 4*) mice after refeeding for 2 h with chow diet. (**B**) Quantification of ^{14}C-labeled free cholesterol in proximal jejunum scrapings of WT (*n = 5*) and B/C KO (*n = 4*) mice 2 h after oral gavage with [^{14}C]cholesterol. (**C**) Gene expression analysis in distal jejunum of WT (*n = 4*) and B/C KO mice (*n = 4*) 2 h after refeeding with western diet + 1.25 % cholesterol. (**D**) Gene expression analysis in distal jejunum of WT (*n = 9*) and BKO (*n = 7*) mice after 4 h of fasting. (**E**) Gene expression analysis in distal jejunum of WT (*n = 10*) and CKO (*n = 7*) mice after 4 h of fasting. (**F**) Gene expression analysis in distal jejunum of F/F (*n = 3*) and I-B KO (*n = 3*) after 4 h fasting. (**G**) Gene expression analysis in distal jejunum of F/F (*n = 4*) and I-C KO (*n = 7*) mice after 4 h of fasting. (**H**) Plasma triglyceride levels in F/F (*n = 4*) and I-B/C KO (*n = 4*) mice after 10 h fasting, followed by refeeding a HC diet for 2 h. (**I**), (**J**) Unlabeled CE (**I**) and unlabeled cholesterol (**J**) in chylomicrons isolated from plasma of F/F (*n = 4*) and I-B/C KO (*n* = 4) mice 3.5 h after treatment with Poloxamer-407 and oral gavage of cholesterol-d4. Data are expressed as mean ± SEM. Statistical analysis: unpaired *t* test; *p < 0.05, **p < 0.01, ***p < 0.001, ****p < 0.0001.

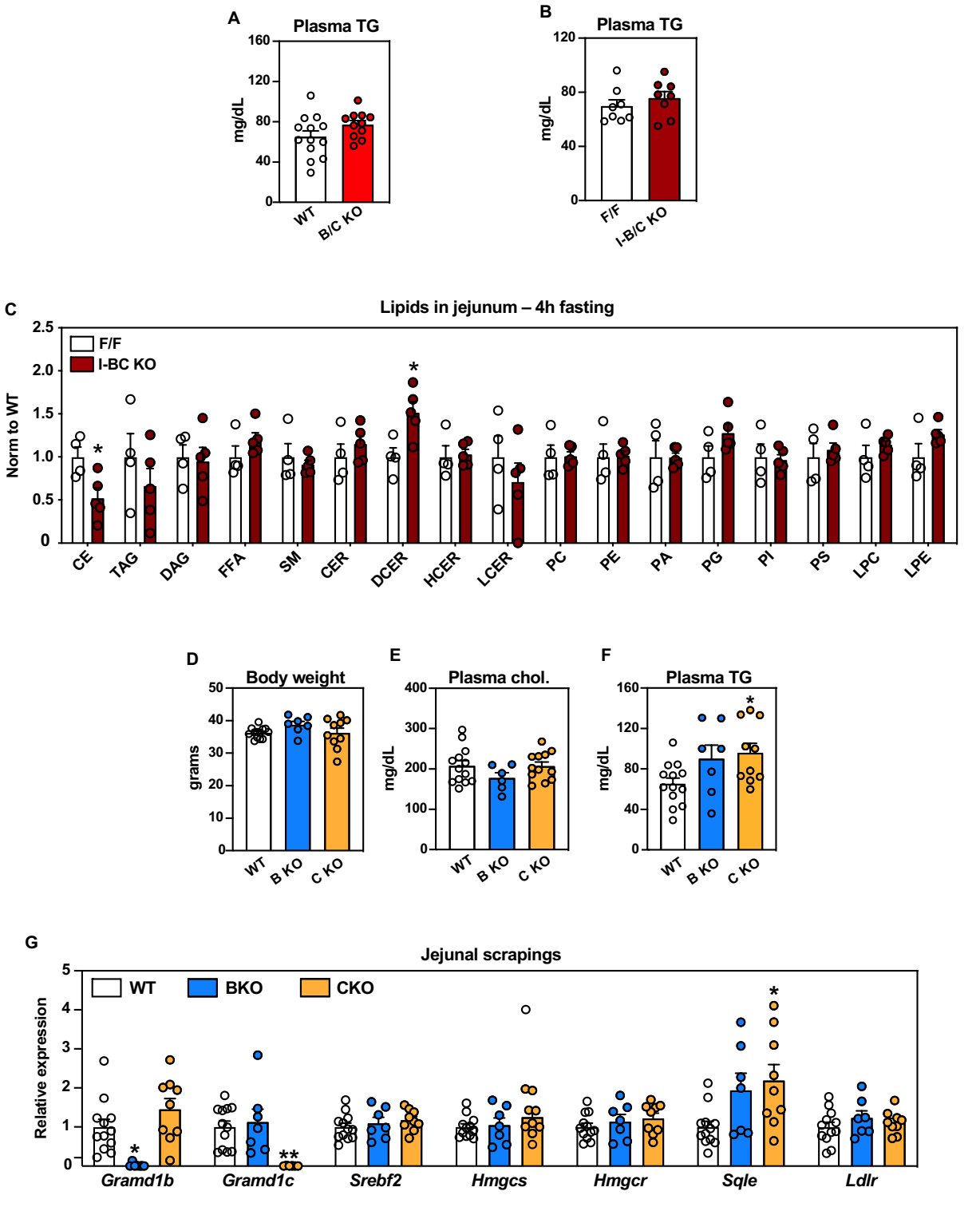

Ferrari et al, Fig. S7

Fig. S7. Global BKO and CKO mice are not protected from diet-induced hypercholesterolemia.

(**A**) Fasting plasma triglycerides in WT (*n = 13*) and B/C KO (*n = 11*) male mice after 21 days of the HC diet. (**B**) Fasting plasma triglycerides in F/F (*n = 17*) and I-B/C KO (*n = 11*) male mice after 21 days on the HC diet. (**C**) Lipidomic analysis from proximal jejunum of F/F (*n = 4*) and I-B/C KO (*n = 5*) male mice fed HC diet for 21 days and euthanized after 4 h of fasting. (**D**) Body weight of WT (*n = 13*), BKO (*n = 7*), and CKO (*n = 10*) mice after 21 days of the HC diet. (**E**) Fasting plasma cholesterol levels in mice described in (D). (**F**) Fasting plasma triglyceride levels for mice described in (D). (**G**) Gene expression in distal jejunum scrapings of mice described in (D). Data are expressed as mean ± SEM. Statistical analysis: unpaired *t* test; *p < 0.05, **p < 0.01.

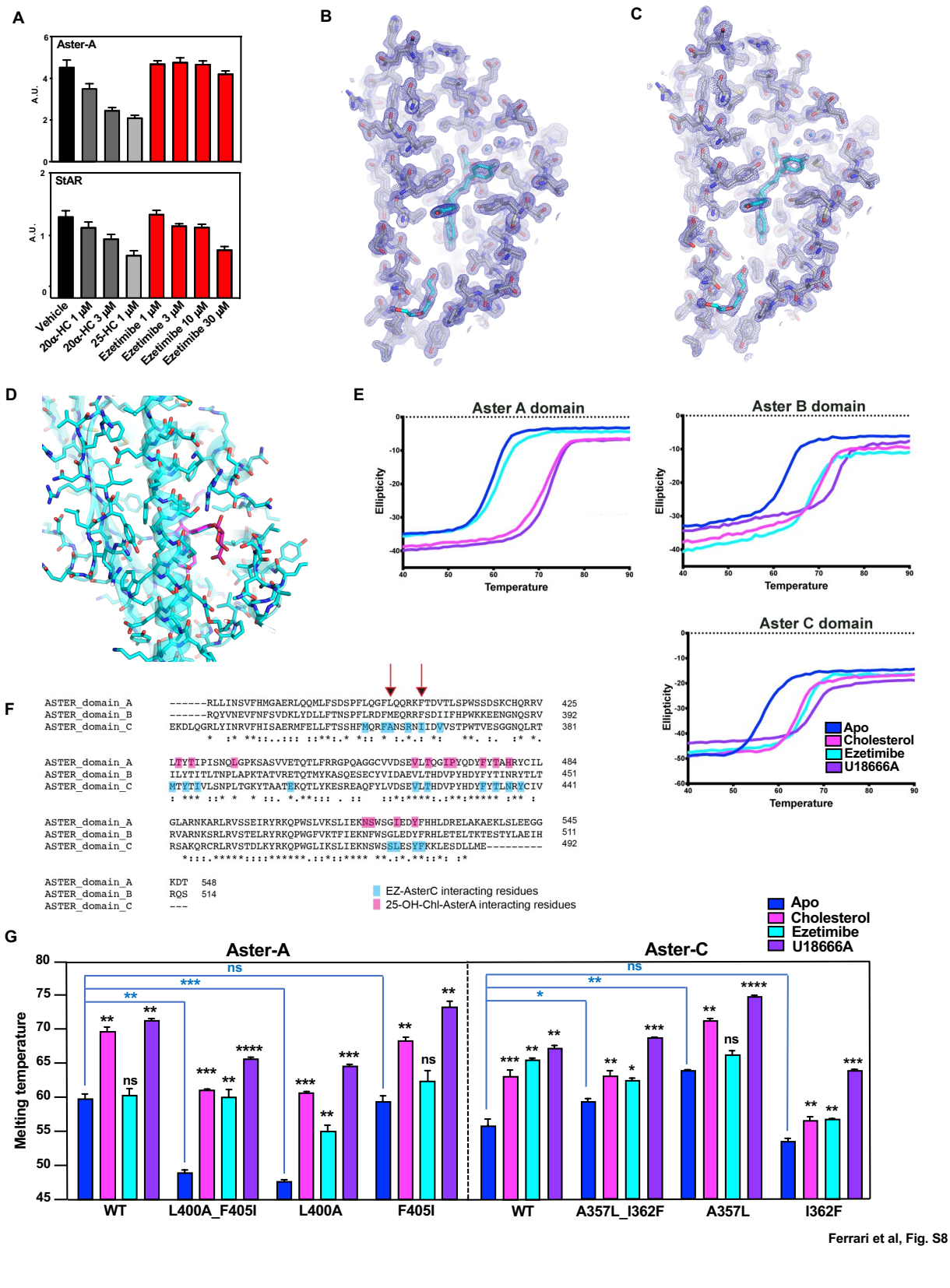

Ferrari et al, Fig. S8

Fig. S8. Selective binding of ASTER-B and -C to ezetimibe.
(**A**) Competition assays for 22-NBD-cholesterol binding to purified ASTER-A and STAR domains incubated in presence of vehicle, 20α-HC, 25-HC, EZ (1–30 mM). Bars represent means ± SD. (**B**) 2Fo-Fc electron density map (contoured at 1.2σ) of Aster-C:EZ showing the ligand EZ along with glycerol and part of PEG 4000 (in sticks), residues surrounding them (in gray sticks), and water molecules (blue spheres) displayed as blue mesh. (**C**) Simulated annealing composite omit map (contoured at 1.2σ of Aster-C:EZ showing EZ, glycerol, and part of PEG 4000 (in sticks), residues surrounding them (in gray sticks), and water molecules (blue spheres) displayed as blue mesh. (**D**) Modeling of ezetimibe-glucuronide in the pocket showing that glucuronide group is oriented toward an opening of the pocket. (**E**) Graphic representation of the ellipticity vs. temperature circular dichroism findings of Aster-A, -B, and -C in the absence of ligand (blue), or in the presence of several ligands (magenta, 25-HC cholesterol; cyan, EZ; purple, U18666A). (**F**) Alignment of Aster-A, -B, and -C domains, highlighting the residues that interact with 25-HC in Aster-A (magenta) and with EZ in Aster-C (cyan). Red arrows point to the main differences in residues involved in ligand interactions in the three proteins. (**G**) Thermal stability of wild-type and mutant Aster-A and -C. The graph shows the melting temperature of the different proteins in the presence or absence of ligands with a statistical comparison between the apo wild-type and the mutants, and between the apo and the ligands within the same protein. Data are expressed as mean ± SEM. Statistical analysis: One-way ANOVA, with Dunnett's post hoc test; *$p < 0.05$, **$p < 0.01$, ***$p < 0.001$, ****$p < 0.0001$.

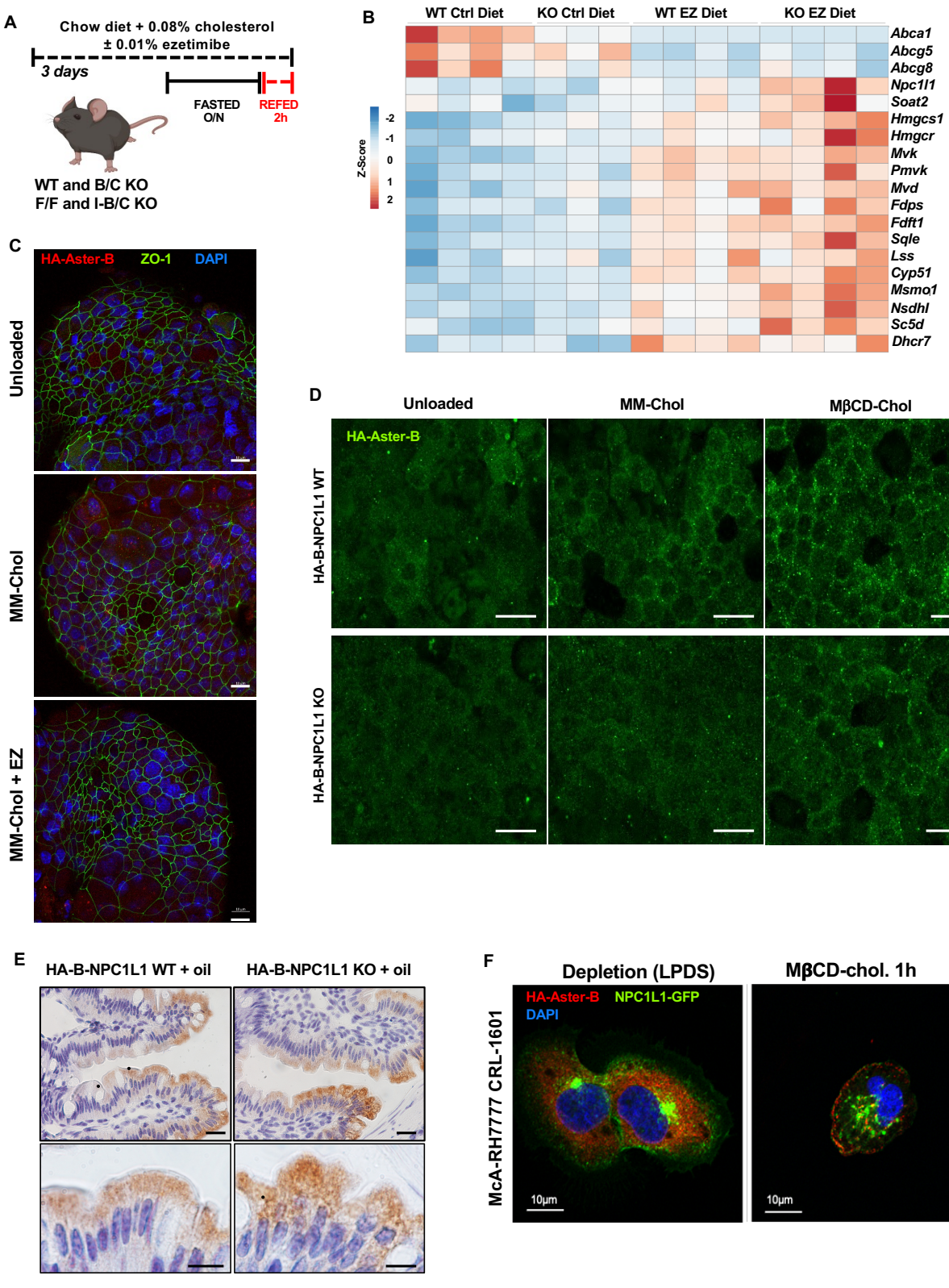

Ferrari et al, Fig. S9

Fig. S9. Mechanism of cooperation between NPC1L1 and Asters.
(**A**) Experimental details for the exposure of WT, B/C KO, F/F, and I-B/C KO mice to a control diet or to a diet containing 0.01% EZ. (**B**) Heatmap showing expression of ABC transporters, *Npc1l1*, *Soat2,* and genes involved in the de novo synthesis of cholesterol in distal jejunum scrapings from WT and B/C KO mice 2 h post refeeding, following 10 h fasting (*n = 3-4*/group). (**C**) Confocal immunofluorescence micrographs of the apical marker ZO-1 and HA-Aster-B in enteroids isolated from 3×HA-Aster-B ileum and grown apical side out, showing recruitment of HA-Aster-B to the apical membrane without cholesterol loading or with cholesterol loading in mixed micelles in presence of vehicle or EZ. Scale bar is 10 mm. (**D**) Immunofluorescence microscopy of HA-Aster-B in intestinal organoids from HA-B-NPC1L1 WT or HA-B-NPC1L1 KO mice during loading with MβCD-cholesterol or cholesterol in mixed micelles. Scale bars 20 mm. (**E**) Immunohistochemistry of HA-Aster-B in small intestines from 3×HA-Aster-B crossed to NPC1L1 WT or NPC1L1 KO mice after a gastric gavage with corn oil. For upper images, scale bar is 20 mm. For lower images, scale bar is 10 mm. (**F**) Confocal imaging and immunofluorescence in a stable cell line expressing NPC1L1-EGFP and HA-Aster-B fusion proteins, during cholesterol depletion by LPDS or MβCD-cholesterol loading. Scale bar is 10 mm.

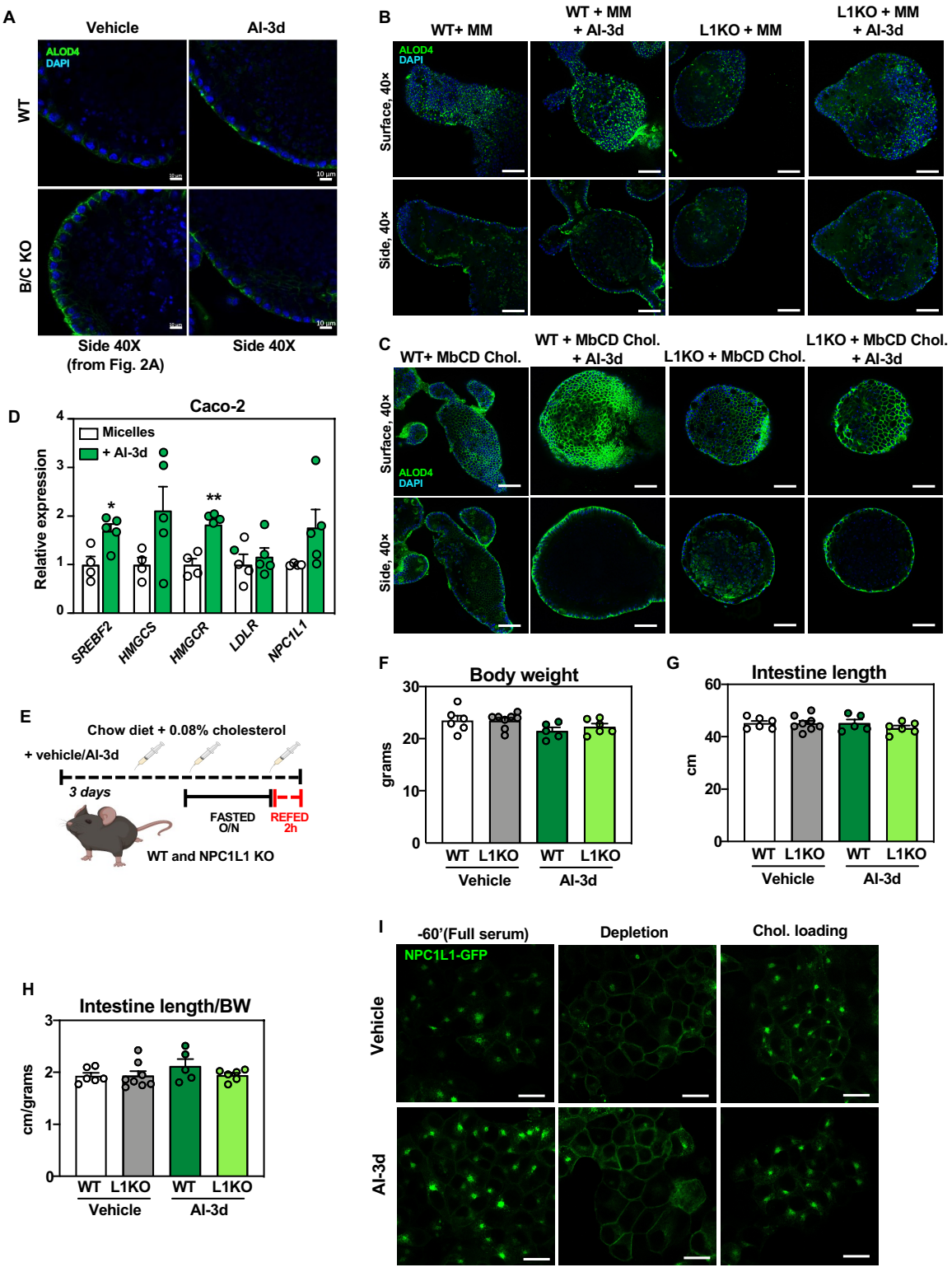

Ferrari et al, Fig. S10

Fig. S10. Pharmacological modulation of Aster function by small molecule inhibitor AI-3d. (**A**) ALOD4 imaging of murine enteroids from WT and B/C KO mice treated with vehicle or AI-3d mice 2 h after loading with MβCD cholesterol. Results presented in this panel and in Fig. 2C came from one experiment, where WT vehicle-treated enteroids served as control for both B/C KO vehicle-treated enteroids and for AI-3d vehicle-treated enteroids. Scale bar is 10 μm. (**B**) ALOD4 imaging of murine enteroids from WT and NPC1L1 KO mice, treated with vehicle or AI-3d, after loading with cholesterol in mixed micelles. Scale bar is 50 μm. (**C**) ALOD4 imaging of murine enteroids from WT and NPC1L1 KO mice, treated with vehicle or AI-3d, after loading or with MβCD-cholesterol. Scale bar is 50 μm. (**D**) Gene expression analysis of SREBP2 and target genes in Caco-2 cells differentiated on transwell and loaded with cholesterol in mixed micelles in the presence of vehicle or AI-3d. (**E**) Experimental details for the exposure of WT and NPC1L1 KO mice to a low cholesterol diet orally gavaged with vehicle or 3 doses of 10 mg/kg AI-3d in corn oil. (**F**) Body weight of mice described in D. (**G**) Intestinal length for mice described in D. (**H**) Intestinal length normalized on body weight for mice described in D. (**I**) McA-RH7777 CRL-1601 hepatocytes stably expressing NPC1L1-EGFP fusion protein, in cells cultured in full serum, after cholesterol depletion with MβCD, or cholesterol depletion with MβCD followed by loading with MβCD-cholesterol for 2 h. Scale bar is 10 μm. Data are expressed as mean ± SEM. Statistical analysis: for panel C, unpaired *t* test; for panels E, F, G, 2-way ANOVA with Tukey's multiple comparisons test $*p < 0.05$, $**p < 0.01$.

Table S1. Antibodies used for detection in immunoblot analyses

Target	Vendor	Cat. number	Dilution	Species
Aster-A	Pierce	Customized antibody	1:1000	Rabbit
Aster-B	Pierce	Customized antibody	1:1000	Rabbit
HA-tag (C29F4)	Cell Signaling	3724S	1:1000 for WB 1:1000 for IF 1:400 for IHC	Rabbit
His-Tag (27E8)	Cell Signaling	2366S	1:1000 for WB 1:400 For IF	Mouse
ApoB	Chemicon	AB742	1:7500	Goat
HMGCR	Millipore	ABS229	1:1000	Rabbit
FDPS	Abcam	ab153805	1:1000	Rabbit
LDL-R	Cayman Chemical	10007665	1:1000	Rabbit
SQLE	Sigma	AV42101	1:1000	Rabbit
CALNEXIN	Abcam	ab10286	1:2000	Rabbit
TUBULIN	Abcam	ab15568	1:10000	Rabbit

Table S2. Primers used for genotyping and mRNA detection by qPCR

Target	Forward	Reverse	Used for
Gramd1b WT	TATTCCAAAAGAGAGGCTGACTTG	ACCAACAGCACACTGACGTC	Genotyping
Gramd1b KO (whole body)	TATTCCAAAAGAGAGGCTGACTTG	AGAGCCCAGATACTAGGTTCAGA	Genotyping
Gramd1c WT	AATGCTGTTTGAGTTGCTGA	GACAAGCAAATATGCACGTGTT	Genotyping
Gramd1c KO (whole body)	AATGCTGTTTGAGTTGCTGA	CCAACTGACCTTGGGCAAGAACAT	Genotyping
Gramd1b flox/flox	AAAGTGTGTTGGTTTAACTCTTGGG	GTTTACAGTCCTAGCCCAAACATC	Genotyping
Gramd1c flox/flox	AATGCTGTTTGAGTTGCTGA	GACAAGCAAATATGCACGTGTT	Genotyping
Cre	GCGGTCTGGCAGTAAAAACTATC	GTGAAACAGCATTGCTGTCACTT	Genotyping
Cre-internal control	CTAGGCCACAGAATTGAAAGATCT	GTAGGTGGAAATTCTAGCATCATCC	Genotyping
Npc1l1 WT	TGTACAAGGAACCCTGACCTCGGG	GCAGAAGCCAGCTTTGTGAGTGGG	Genotyping
Npc1l1 KO	TGTACAAGGAACCCTGACCTCGGG	CAACGGGTTCTTCTGTTAGTCC	Genotyping
3xHA-Aster-B	GAAAGAATATCGGCCGGGGT	GGCCAAAGAGTTCTGGCTCA	Genotyping
36b4	GGCCCTGCACTCTCGCTTTC	TGCCAGGACGCGCTTGT	qPCR
Gramd1a	CAGCAGATGCTCTTCTCGGA	TCTGAGGATACACGAAGCCG	qPCR
Gramd1b	TCCCAATGCCATCCAAGTC	ACAAAGTGCCAGAGCTCC	qPCR
Gramd1c	CCGTGTCTTTCACATCAGTGC	ACTTCCCAGTTAGCGGGTTG	qPCR
Srebf2	ACCTAGACCTCGCCAAAGGT	GCACGGATAAGCAGGTTTGT	qPCR
Hmgcs	GCCGTGAACTGGGTCGAA	GCATATATAGCAATGTCTCCT	qPCR
Hmgcr	CTTGTGGAATGCCTTGTGATT	AGCCGAAGCAGCACATGAT	qPCR
Sqle	GCCTCTCAGAATGGTCGTCT	CGCATGTCCCAGAATAAGGA	qPCR
Ldlr	AGGCTGTGGGCTCCATAGG	TGCGGTCCAGGGTCATCT	qPCR
Abca1	GGTTTGGAGATGGTTATACAATAG TTGT	TTCCCGGAAACGCAAGTC	qPCR
Soat2	ACTGTGCCTGGGATCTTTTG	ACATAGTTCCACCTGATGCTG	qPCR
Npc1l1	CAACATCTTCATCTTTGTTCTTGAG	GCCAATGTGAGCCTCTCG	qPCR
Idol	AGGAGATCAACTCCACCTTCTG	ATCTGCAGACCGGACAGG	qPCR
Lpcat3	GGCCTCTCAATTGCTTATTTCA	AGCACGACACATAGCAAGGA	
36B4	CCACGCTGCTGAACATGCT	TCGAACACCTGCTGGATGAC	qPCR
GRAMD1A	CAAGATGCTGAGCCCCACTT	GGCGCAGGAGTAATCCACAA	qPCR
GRAMD1B	TGACCAGATGAAGGACTCGCT	ACTTTCCGACGTGTAGTCGC	qPCR
GRAMD1C	ACCTTCAACCGAACAGCAGA	TTCCATTTCCTTTTTCTTTCCTGTA	qPCR
SQLE	TCCTTGCTCAGGCTCTTTATG	AGGGTTAGGAGACAATACAGAAAG	qPCR
SREBF2	ATCTGGATCTCGCCAGAGG	CCAGGCAGGTTTGTAGGTTG	qPCR
HMGCS	TTCGTGGCTCACTCCCTTT	CTGTCACTGTTTCCTCCTTCG	qPCR
HMGCR	GACGCAACCTTTATATCCGTT	TTGAAACTGCTTTCTCTGTAC	qPCR
LDLR	AGGACGGCTACAGCTACCC	CTCCAGGCAGATGTTCACG	qPCR
NPC1L1	GACCATTTTCTGTACTGTGCC	CTGCCTCAGAATAGTCCTTTCC	qPCR
ALPI	GCCAACTTCCAGACCATCG	CCACTCCTACTGACTTTCCTG	qPCR
MTTP	TCAGAAACTTCCTGGCCTTC	AATGGCTTCTAATGAGTCTGAGG	qPCR

Table S3. Data collection and refinement statistics for the crystal structure of Aster-C with ezetimibe.

Wavelength	0.9686
Resolution range	40.93 - 1.6 (1.657 - 1.6)
Space group	P 4_1 2_1 2
Unit cell	49.62 49.62 144.77 90 90 90
Total reflections	552,892 (27,706)
Unique reflections	24,703 (2,330)
Multiplicity	22.4 (11.9)
Completeness (%)	99.6 (96.5)
Mean I/sigma(I)	30.3 (2.5)
Wilson B-factor	18
R-merge	0.295 (0.529)
R-meas	0.302 (0.553)
R-pim	0.061 (0.154)
CC1/2	0.976 (0.894)
CC*	0.994 (0.972)
Reflections used in refinement	24,702 (2,330)
Reflections used for R-free	1,245 (129)
R-work	0.1724 (0.1933)
R-free	0.2059 (0.2365)
CC(work)	0.961 (0.919)
CC(free)	0.937 (0.919)
Number of non-hydrogen atoms	1666
macromolecules	1433
ligands	140
solvent	168
Protein residues	171
RMS(bonds)	0.012
RMS(angles)	1.15
Ramachandran favored (%)	98.82
Ramachandran allowed (%)	1.18
Ramachandran outliers (%)	0.00
Rotamer outliers (%)	0.00
Clashscore	4.04
Average B-factor	23
macromolecules	22
ligands	33
solvent	32

References and Notes

1. P. Xie, H. Zhu, L. Jia, Y. Ma, W. Tang, Y. Wang, B. Xue, H. Shi, L. Yu, Genetic demonstration of intestinal NPC1L1 as a major determinant of hepatic cholesterol and blood atherogenic lipoprotein levels. *Atherosclerosis* **237**, 609–617 (2014). doi:10.1016/j.atherosclerosis.2014.09.036 Medline

2. C. M. Mansbach, S. A. Siddiqi, The biogenesis of chylomicrons. *Annu. Rev. Physiol.* **72**, 315–333 (2010). doi:10.1146/annurev-physiol-021909-135801 Medline

3. K. K. Buhman, M. Accad, S. Novak, R. S. Choi, J. S. Wong, R. L. Hamilton, S. Turley, R. V. Farese Jr., Resistance to diet-induced hypercholesterolemia and gallstone formation in ACAT2-deficient mice. *Nat. Med.* **6**, 1341–1347 (2000). doi:10.1038/82153 Medline

4. T. M. Nguyen, J. K. Sawyer, K. L. Kelley, M. A. Davis, L. L. Rudel, Cholesterol esterification by ACAT2 is essential for efficient intestinal cholesterol absorption: Evidence from thoracic lymph duct cannulation. *J. Lipid Res.* **53**, 95–104 (2012). doi:10.1194/jlr.M018820 Medline

5. J. Zhang, K. L. Kelley, S. M. Marshall, M. A. Davis, M. D. Wilson, J. K. Sawyer, R. V. Farese Jr., J. M. Brown, L. L. Rudel, Tissue-specific knockouts of ACAT2 reveal that intestinal depletion is sufficient to prevent diet-induced cholesterol accumulation in the liver and blood. *J. Lipid Res.* **53**, 1144–1152 (2012). doi:10.1194/jlr.M024356 Medline

6. S. W. Altmann, H. R. Davis Jr., L. J. Zhu, X. Yao, L. M. Hoos, G. Tetzloff, S. P. Iyer, M. Maguire, A. Golovko, M. Zeng, L. Wang, N. Murgolo, M. P. Graziano, Niemann-Pick C1 Like 1 protein is critical for intestinal cholesterol absorption. *Science* **303**, 1201–1204 (2004). doi:10.1126/science.1093131 Medline

7. H. R. Davis Jr., L. J. Zhu, L. M. Hoos, G. Tetzloff, M. Maguire, J. Liu, X. Yao, S. P. N. Iyer, M.-H. Lam, E. G. Lund, P. A. Detmers, M. P. Graziano, S. W. Altmann, Niemann-Pick C1 Like 1 (NPC1L1) is the intestinal phytosterol and cholesterol transporter and a key modulator of whole-body cholesterol homeostasis. *J. Biol. Chem.* **279**, 33586–33592 (2004). doi:10.1074/jbc.M405817200 Medline

8. M. Garcia-Calvo, J. Lisnock, H. G. Bull, B. E. Hawes, D. A. Burnett, M. P. Braun, J. H. Crona, H. R. Davis Jr., D. C. Dean, P. A. Detmers, M. P. Graziano, M. Hughes, D. E. Macintyre, A. Ogawa, K. A. O'neill, S. P. N. Iyer, D. E. Shevell, M. M. Smith, Y. S. Tang, A. M. Makarewicz, F. Ujjainwalla, S. W. Altmann, K. T. Chapman, N. A. Thornberry, The target of ezetimibe is Niemann-Pick C1-Like 1 (NPC1L1). *Proc. Natl. Acad. Sci. U.S.A.* **102**, 8132–8137 (2005). doi:10.1073/pnas.0500269102 Medline

9. H. R. Davis Jr., K. K. Pula, K. B. Alton, R. E. Burrier, R. W. Watkins, The synergistic hypocholesterolemic activity of the potent cholesterol absorption inhibitor, ezetimibe, in combination with 3-hydroxy-3-methylglutaryl coenzyme a reductase inhibitors in dogs. *Metabolism* **50**, 1234–1241 (2001). doi:10.1053/meta.2001.26737 Medline

10. C. P. Cannon, M. A. Blazing, R. P. Giugliano, A. McCagg, J. A. White, P. Theroux, H. Darius, B. S. Lewis, T. O. Ophuis, J. W. Jukema, G. M. De Ferrari, W. Ruzyllo, P. De Lucca, K. Im, E. A. Bohula, C. Reist, S. D. Wiviott, A. M. Tershakovec, T. A. Musliner, E. Braunwald, R. M. Califf; IMPROVE-IT Investigators, Ezetimibe Added to Statin

Therapy after Acute Coronary Syndromes. *N. Engl. J. Med.* **372**, 2387–2397 (2015). doi:10.1056/NEJMoa1410489 Medline

11. J. W. Clader, The discovery of ezetimibe: A view from outside the receptor. *J. Med. Chem.* **47**, 1–9 (2004). doi:10.1021/jm030283g Medline

12. H. R. Davis Jr., D. S. Compton, L. Hoos, G. Tetzloff, Ezetimibe, a potent cholesterol absorption inhibitor, inhibits the development of atherosclerosis in ApoE knockout mice. *Arterioscler. Thromb. Vasc. Biol.* **21**, 2032–2038 (2001). doi:10.1161/hq1201.100260 Medline

13. R. G. Lee, K. L. Kelley, J. K. Sawyer, R. V. Farese Jr., J. S. Parks, L. L. Rudel, Plasma cholesteryl esters provided by lecithin:cholesterol acyltransferase and acyl-coenzyme a:cholesterol acyltransferase 2 have opposite atherosclerotic potential. *Circ. Res.* **95**, 998–1004 (2004). doi:10.1161/01.RES.0000147558.15554.67 Medline

14. M. Hu, F. Yang, Y. Huang, X. You, D. Liu, S. Sun, S.-F. Sui, Structural insights into the mechanism of human NPC1L1-mediated cholesterol uptake. *Sci. Adv.* **7**, eabg3188 (2021). doi:10.1126/sciadv.abg3188 Medline

15. C.-S. Huang, X. Yu, P. Fordstrom, K. Choi, B. C. Chung, S-H. Roh, W. Chiu, M. Zhou, X. Min, Z. Wang, Cryo-EM structures of NPC1L1 reveal mechanisms of cholesterol transport and ezetimibe inhibition. *Sci. Adv.* **6**, eabb1989 (2020). doi:10.1126/sciadv.abb1989 Medline.

16. T. Long, Y. Liu, Y. Qin, R. A. DeBose-Boyd, X. Li, Structures of dimeric human NPC1L1 provide insight into mechanisms for cholesterol absorption. *Sci. Adv.* **7**, eabh3997 (2021). doi:10.1126/sciadv.abh3997 Medline

17. L. Ge, J. Wang, W. Qi, H.-H. Miao, J. Cao, Y.-X. Qu, B.-L. Li, B.-L. Song, The cholesterol absorption inhibitor ezetimibe acts by blocking the sterol-induced internalization of NPC1L1. *Cell Metab.* **7**, 508–519 (2008). doi:10.1016/j.cmet.2008.04.001 Medline

18. A. B. Weinglass, M. Kohler, U. Schulte, J. Liu, E. O. Nketiah, A. Thomas, W. Schmalhofer, B. Williams, W. Bildl, D. R. McMasters, K. Dai, L. Beers, M. E. McCann, G. J. Kaczorowski, M. L. Garcia, Extracellular loop C of NPC1L1 is important for binding to ezetimibe. *Proc. Natl. Acad. Sci. U.S.A.* **105**, 11140–11145 (2008). doi:10.1073/pnas.0800936105 Medline

19. L. Ge, W. Qi, L.-J. Wang, H.-H. Miao, Y.-X. Qu, B.-L. Li, B.-L. Song, Flotillins play an essential role in Niemann-Pick C1-like 1-mediated cholesterol uptake. *Proc. Natl. Acad. Sci. U.S.A.* **108**, 551–556 (2011). doi:10.1073/pnas.1014434108 Medline

20. L.-J. Wang, J. Wang, N. Li, L. Ge, B. L. Li, B. L. Song, Molecular characterization of the NPC1L1 variants identified from cholesterol low absorbers. *J. Biol. Chem.* **286**, 7397–7408 (2011). doi:10.1074/jbc.M110.178368 Medline

21. P.-S. Li, Z.-Y. Fu, Y.-Y. Zhang, J.-H. Zhang, C.-Q. Xu, Y.-T. Ma, B.-L. Li, B.-L. Song, The clathrin adaptor Numb regulates intestinal cholesterol absorption through dynamic interaction with NPC1L1. *Nat. Med.* **20**, 80–86 (2014). doi:10.1038/nm.3417 Medline

22. B.-B. Chu, L. Ge, C. Xie, Y. Zhao, H.-H. Miao, J. Wang, B.-L. Li, B.-L. Song, Requirement of myosin Vb.Rab11a.Rab11-FIP2 complex in cholesterol-regulated translocation of

NPC1L1 to the cell surface. *J. Biol. Chem.* **284**, 22481–22490 (2009). doi:10.1074/jbc.M109.034355 Medline

23. T. A. Johnson, S. R. Pfeffer, Ezetimibe-sensitive cholesterol uptake by NPC1L1 protein does not require endocytosis. *Mol. Biol. Cell* **27**, 1845–1852 (2016). doi:10.1091/mbc.e16-03-0154 Medline

24. Y.-Y. Zhang, Z.-Y. Fu, J. Wei, W. Qi, G. Baituola, J. Luo, Y.-J. Meng, S.-Y. Guo, H. Yin, S.-Y. Jiang, Y.-F. Li, H.-H. Miao, Y. Liu, Y. Wang, B.-L. Li, Y.-T. Ma, B.-L. Song, A *LIMA1* variant promotes low plasma LDL cholesterol and decreases intestinal cholesterol absorption. *Science* **360**, 1087–1092 (2018). doi:10.1126/science.aao6575 Medline

25. J. Sandhu, S. Li, L. Fairall, S. G. Pfisterer, J. E. Gurnett, X. Xiao, T. A. Weston, D. Vashi, A. Ferrari, J. L. Orozco, C. L. Hartman, D. Strugatsky, S. D. Lee, C. He, C. Hong, H. Jiang, L. A. Bentolila, A. T. Gatta, T. P. Levine, A. Ferng, R. Lee, D. A. Ford, S. G. Young, E. Ikonen, J. W. R. Schwabe, P. Tontonoz, Aster Proteins Facilitate Nonvesicular Plasma Membrane to ER Cholesterol Transport in Mammalian Cells. *Cell* **175**, 514–529.e20 (2018). doi:10.1016/j.cell.2018.08.033 Medline

26. T. Naito, B. Ercan, L. Krshnan, A. Triebl, D. H. Z. Koh, F.-Y. Wei, K. Tomizawa, F. T. Torta, M. R. Wenk, Y. Saheki, Movement of accessible plasma membrane cholesterol by the GRAMD1 lipid transfer protein complex. *eLife* **8**, e51401 (2019). doi:10.7554/eLife.51401 Medline

27. M. Besprozvannaya, E. Dickson, H. Li, K. S. Ginburg, D. M. Bers, J. Auwerx, J. Nunnari, GRAM domain proteins specialize functionally distinct ER-PM contact sites in human cells. *eLife* **7**, e31019 (2018). doi:10.7554/eLife.31019 Medline

28. X. Xiao, J. P. Kennelly, A. Ferrari, B. L. Clifford, E. Whang, Y. Gao, K. Qian, J. Sandhu, K. E. Jarrett, M. C. Brearley-Sholto, A. Nguyen, R. T. Nagari, M. S. Lee, S. Zhang, T. A. Weston, S. G. Young, S. J. Bensinger, C. J. Villanueva, T. Q. de Aguiar Vallim, P. Tontonoz, Hepatic nonvesicular cholesterol transport is critical for systemic lipid homeostasis. *Nat. Metab.* **5**, 165–181 (2023). doi:10.1038/s42255-022-00722-6 Medline

29. B. Wang, P. Tontonoz, Liver X receptors in lipid signalling and membrane homeostasis. *Nat. Rev. Endocrinol.* **14**, 452–463 (2018). doi:10.1038/s41574-018-0037-x Medline

30. L. Yu, S. Gupta, F. Xu, A. D. B. Liverman, A. Moschetta, D. J. Mangelsdorf, J. J. Repa, H. H. Hobbs, J. C. Cohen, Expression of ABCG5 and ABCG8 is required for regulation of biliary cholesterol secretion. *J. Biol. Chem.* **280**, 8742–8747 (2005). doi:10.1074/jbc.M411080200 Medline

31. H. Jiang, C. N. Goulbourne, A. Tatar, K. Turlo, D. Wu, A. P. Beigneux, C. R. M. Grovenor, L. G. Fong, S. G. Young, High-resolution imaging of dietary lipids in cells and tissues by NanoSIMS analysis. *J. Lipid Res.* **55**, 2156–2166 (2014). doi:10.1194/jlr.M053363 Medline

32. C. He, T. A. Weston, R. S. Jung, P. Heizer, M. Larsson, X. Hu, C. M. Allan, P. Tontonoz, K. Reue, A. P. Beigneux, M. Ploug, A. Holme, M. Kilburn, P. Guagliardo, D. A. Ford, L. G. Fong, S. G. Young, H. Jiang, NanoSIMS Analysis of Intravascular Lipolysis and Lipid Movement across Capillaries and into Cardiomyocytes. *Cell Metab.* **27**, 1055–1066.e3 (2018). doi:10.1016/j.cmet.2018.03.017 Medline

33. A. Ferrari, C. He, J. P. Kennelly, J. Sandhu, X. Xiao, X. Chi, H. Jiang, S. G. Young, P. Tontonoz, Aster Proteins Regulate the Accessible Cholesterol Pool in the Plasma Membrane. *Mol. Cell. Biol.* **40**, e00255–e00220 (2020). doi:10.1128/MCB.00255-20 Medline

34. A. Das, M. S. Brown, D. D. Anderson, J. L. Goldstein, A. Radhakrishnan, Three pools of plasma membrane cholesterol and their relation to cholesterol homeostasis. *eLife* **40**, e02882 (2014). doi:10.1128/MCB.00255-20 Medline

35. A. Gay, D. Rye, A. Radhakrishnan, Switch-like responses of two cholesterol sensors do not require protein oligomerization in membranes. *Biophys. J.* **108**, 1459–1469 (2015). doi:10.1016/j.bpj.2015.02.008 Medline

36. X. Xiao, Y. Kim, B. Romartinez-Alonso, K. Sirvydis, D. S. Ory, J. W. R. Schwabe, M. E. Jung, P. Tontonoz, Selective Aster inhibitors distinguish vesicular and nonvesicular sterol transport mechanisms. *Proc. Natl. Acad. Sci. U.S.A.* **118**, e2024149118 (2021). doi:10.1073/pnas.2024149118 Medline

37. J. Y. Co, M. Margalef-Català, X. Li, A. T. Mah, C. J. Kuo, D. M. Monack, M. R. Amieva, Controlling Epithelial Polarity: A Human Enteroid Model for Host-Pathogen Interactions. *Cell Rep.* **26**, 2509–2520.e4 (2019). doi:10.1016/j.celrep.2019.01.108 Medline

38. C. Xie, Z. S. Zhou, N. Li, Y. Bian, Y. J. Wang, L. J. Wang, B. L. Li, B. L. Song, Ezetimibe blocks the internalization of NPC1L1 and cholesterol in mouse small intestine. *J. Lipid Res.* **53**, 2092–2101 (2012). doi:10.1194/jlr.M027359 Medline

39. E. D. Carstea, J. A. Morris, K. G. Coleman, S. K. Loftus, D. Zhang, C. Cummings, J. Gu, M. A. Rosenfeld, W. J. Pavan, D. B. Krizman, J. Nagle, M. H. Polymeropoulos, S. L. Sturley, Y. A. Ioannou, M. E. Higgins, M. Comly, A. Cooney, A. Brown, C. R. Kaneski, E. J. Blanchette-Mackie, N. K. Dwyer, E. B. Neufeld, T.-Y. Chang, L. Liscum, J. F. Strauss 3rd, K. Ohno, M. Zeigler, R. Carmi, J. Sokol, D. Markie, R. R. O'Neill, O. P. van Diggelen, M. Elleder, M. C. Patterson, R. O. Brady, M. T. Vanier, P. G. Pentchev, D. A. Tagle, Niemann-Pick C1 disease gene: Homology to mediators of cholesterol homeostasis. *Science* **277**, 228–231 (1997). doi:10.1126/science.277.5323.228 Medline

40. H. J. Kwon, L. Abi-Mosleh, M. L. Wang, J. Deisenhofer, J. L. Goldstein, M. S. Brown, R. E. Infante, Structure of N-terminal domain of NPC1 reveals distinct subdomains for binding and transfer of cholesterol. *Cell* **137**, 1213–1224 (2009). doi:10.1016/j.cell.2009.03.049 Medline

41. H. Qian, X. Wu, X. Du, X. Yao, X. Zhao, J. Lee, H. Yang, N. Yan, Structural Basis of Low-pH-Dependent Lysosomal Cholesterol Egress by NPC1 and NPC2. *Cell* **182**, 98–111.e18 (2020). doi:10.1016/j.cell.2020.05.020 Medline

42. H. Wang, Q. Ma, Y. Qi, J. Dong, X. Du, J. Rae, J. Wang, W.-F. Wu, A. J. Brown, R. G. Parton, J.-W. Wu, H. Yang, ORP2 Delivers Cholesterol to the Plasma Membrane in Exchange for Phosphatidylinositol 4, 5-Bisphosphate (PI(4,5)P_2). *Mol. Cell* **73**, 458–473.e7 (2019). doi:10.1016/j.molcel.2018.11.014 Medline

43.Materials and methods are available as supplementary materials.

R44. B. Wang, X. Rong, M. A. Duerr, D. J. Hermanson, P. N. Hedde, J. S. Wong, T. Q. Vallim, B. F. Cravatt, E. Gratton, D. A. Ford, P. Tontonoz, Intestinal Phospholipid Remodeling Is

Required for Dietary-Lipid Uptake and Survival on a High-Fat Diet. *Cell Metab.* **23**, 492–504 (2016). doi:10.1016/j.cmet.2016.01.001 Medline

45. S. D. Lee, S. J. Thornton, K. Sachs-Barrable, J. H. Kim, K. M. Wasan, Evaluation of the contribution of the ATP binding cassette transporter, P-glycoprotein, to in vivo cholesterol homeostasis. *Mol. Pharm.* **10**, 3203–3212 (2013). doi:10.1021/mp4002415 Medline

46. J. Folch, M. Lees, G. H. Sloane Stanley, A simple method for the isolation and purification of total lipides from animal tissues. *J. Biol. Chem.* **226**, 497–509 (1957). doi:10.1016/S0021-9258(18)64849-5 Medline

47. E. G. Bligh, W. J. Dyer, A rapid method of total lipid extraction and purification. *Can. J. Biochem. Physiol.* **37**, 911–917 (1959). doi:10.1139/y59-099 Medline

48. A. M. Bolger, M. Lohse, B. Usadel, Trimmomatic: A flexible trimmer for Illumina sequence data. *Bioinformatics* **30**, 2114–2120 (2014). doi:10.1093/bioinformatics/btu170 Medline

49. A. Dobin, C. A. Davis, F. Schlesinger, J. Drenkow, C. Zaleski, S. Jha, P. Batut, M. Chaisson, T. R. Gingeras, STAR: Ultrafast universal RNA-seq aligner. *Bioinformatics* **29**, 15–21 (2013). doi:10.1093/bioinformatics/bts635 Medline

50. S. Anders, P. T. Pyl, W. Huber, HTSeq—A Python framework to work with high-throughput sequencing data. *Bioinformatics* **31**, 166–169 (2015). doi:10.1093/bioinformatics/btu638 Medline

51. M. I. Love, W. Huber, S. Anders, Moderated estimation of fold change and dispersion for RNA-seq data with DESeq2. *Genome Biol.* **15**, 550 (2014). doi:10.1186/s13059-014-0550-8 Medline

52. W.-Y. Hsieh, Q. D. Zhou, A. G. York, K. J. Williams, P. O. Scumpia, E. B. Kronenberger, X. P. Hoi, B. Su, X. Chi, V. L. Bui, E. Khialeeva, A. Kaplan, Y. M. Son, A. S. Divakaruni, J. Sun, S. T. Smale, R. A. Flavell, S. J. Bensinger, Toll-Like Receptors Induce Signal-Specific Reprogramming of the Macrophage Lipidome. *Cell Metab.* **32**, 128–143.e5 (2020). doi:10.1016/j.cmet.2020.05.003 Medline

53. B. Su, L. F. Bettcher, W.-Y. Hsieh, D. Hornburg, M. J. Pearson, N. Blomberg, M. Giera, M. P. Snyder, D. Raftery, S. J. Bensinger, K. J. Williams, A DMS Shotgun Lipidomics Workflow Application to Facilitate High-Throughput, Comprehensive Lipidomics. *J. Am. Soc. Mass Spectrom.* **32**, 2655–2663 (2021). doi:10.1021/jasms.1c00203 Medline

54. G. Liebisch, M. Binder, R. Schifferer, T. Langmann, B. Schulz, G. Schmitz, High throughput quantification of cholesterol and cholesteryl ester by electrospray ionization tandem mass spectrometry (ESI-MS/MS). *Biochim. Biophys. Acta* **1761**, 121–128 (2006). doi:10.1016/j.bbalip.2005.12.007 Medline

55. S. Preibisch, S. Saalfeld, P. Tomancak, Globally optimal stitching of tiled 3D microscopic image acquisitions. *Bioinformatics* **25**, 1463–1465 (2009). doi:10.1093/bioinformatics/btp184 Medline

56. T. Sato, R. G. Vries, H. J. Snippert, M. van de Wetering, N. Barker, D. E. Stange, J. H. van Es, A. Abo, P. Kujala, P. J. Peters, H. Clevers, Single Lgr5 stem cells build crypt-villus

structures in vitro without a mesenchymal niche. *Nature* **459**, 262–265 (2009). doi:10.1038/nature07935 Medline

57. H. Miyoshi, T. S. Stappenbeck, In vitro expansion and genetic modification of gastrointestinal stem cells in spheroid culture. *Nat. Protoc.* **8**, 2471–2482 (2013). doi:10.1038/nprot.2013.153 Medline

58. S. Endapally, R. E. Infante, A. Radhakrishnan, in *Intracellular Lipid Transport: Methods and Protocols*, G. Drin, Ed. (Springer, 2019), pp. 153-163.

59. G. Winter, xia2: An expert system for macromolecular crystallography data reduction. *J. Appl. Cryst.* **43**, 186–190 (2010). doi:10.1107/S0021889809045701

60. P. R. Evans, G. N. Murshudov, How good are my data and what is the resolution? *Acta Crystallogr. D.* **69**, 1204–1214 (2013). doi:10.1107/S0907444913000061 Medline

61. M. D. Winn, C. C. Ballard, K. D. Cowtan, E. J. Dodson, P. Emsley, P. R. Evans, R. M. Keegan, E. B. Krissinel, A. G. W. Leslie, A. McCoy, S. J. McNicholas, G. N. Murshudov, N. S. Pannu, E. A. Potterton, H. R. Powell, R. J. Read, A. Vagin, K. S. Wilson, Overview of the CCP4 suite and current developments. *Acta Crystallogr. D.* **67**, 235–242 (2011). doi:10.1107/S0907444910045749 Medline

62. A. J. McCoy, R. D. Oeffner, A. G. Wrobel, J. R. M. Ojala, K. Tryggvason, B. Lohkamp, R. J. Read, Ab initio solution of macromolecular crystal structures without direct methods. *Proc. Natl. Acad. Sci. U.S.A.* **114**, 3637–3641 (2017). doi:10.1073/pnas.1701640114 Medline

63. P. Emsley, B. Lohkamp, W. G. Scott, K. Cowtan, Features and development of Coot. *Acta Crystallogr. D.* **66**, 486–501 (2010). doi:10.1107/S0907444910007493 Medline

64. G. G. Langer, S. Hazledine, T. Wiegels, C. Carolan, V. S. Lamzin, Visual automated macromolecular model building. *Acta Crystallogr. D.* **69**, 635–641 (2013). doi:10.1107/S0907444913000565 Medline

65. G. N. Murshudov, P. Skubák, A. A. Lebedev, N. S. Pannu, R. A. Steiner, R. A. Nicholls, M. D. Winn, F. Long, A. A. Vagin, REFMAC5 for the refinement of macromolecular crystal structures. *Acta Crystallogr. D.* **67**, 355–367 (2011). doi:10.1107/S0907444911001314 Medline

66. D. Liebschner, P. V. Afonine, M. L. Baker, G. Bunkóczi, V. B. Chen, T. I. Croll, B. Hintze, L.-W. Hung, S. Jain, A. J. McCoy, N. W. Moriarty, R. D. Oeffner, B. K. Poon, M. G. Prisant, R. J. Read, J. S. Richardson, D. C. Richardson, M. D. Sammito, O. V. Sobolev, D. H. Stockwell, T. C. Terwilliger, A. G. Urzhumtsev, L. L. Videau, C. J. Williams, P. D. Adams, Macromolecular structure determination using X-rays, neutrons and electrons: Recent developments in Phenix. *Acta Crystallogr. D.* **75**, 861–877 (2019). doi:10.1107/S2059798319011471 Medline